J. Fluid Mech. (1983), *vol.* 130, *pp.* 315–345
Printed in Great Britain

Steady and unsteady separation in an approximately two-dimensional indented channel

By C. D. BERTRAM† AND T. J. PEDLEY

Department of Applied Mathematics and Theoretical Physics, University of Cambridge, Silver Street, Cambridge CB3 9EW

(Received 4 August 1981 and in revised form 17 December 1982)

Experiments are performed on steady and impulsively started flow in an approximately two-dimensional closed channel, with one wall locally indented. In plan the indentation is a long trapezium which halves the channel width; the inclination of the sloping walls is approximately 5.7°, and these tapered sections merge smoothly into the narrowest section via rounded corners. The Reynolds number $Re = a_0\bar{u}_0/\nu$ (a_0 = unindented channel width, $\bar{u}_0$ = steady mean velocity in the unindented channel) lies in the range $300 \leqslant Re \leqslant 1800$. In steady flow, flow visualization reveals that separation occurs on the lee slope of the indentation, at a distance downstream of the convex corner which decreases (tending to a non-zero value) as Re increases. There is no upstream separation, and there is some evidence of three-dimensionality of the flow in the downstream separated eddy. Pressure measurements agree qualitatively but not quantitatively with theoretical predictions. Unsteady flow visualization reveals that, as in external flow, wall-shear reversal occurs over much of the lee slope (at dimensionless time $\tau = \bar{u}_0 t/a_0 \approx 4$) before there is any evidence of severe boundary-layer thickening and breakaway. Then, at $\tau \approx 5.5$, a separated eddy develops, and its nose moves gradually upstream from the downstream end of the indentation to its eventual ($\tau \approx 75$) steady-state position on the lee slope. At about the same time as the wall-shear reversal, wavy vortices appear at the edge of the boundary layer on both walls of the channel, and (for $Re < 750$) subsequently disappear again; these are interpreted as manifestations of inflection-point instability and not as intrinsic aspects of boundary-layer separation. Pressure measurements are made to investigate the discrepancy between the actual pressure drop across the lee slope and that predicted on the assumption that energy dissipation is quasi-steady. This discrepancy has a maximum value of approximately $1.5\rho\bar{u}_0^2$ (ρ = fluid density), and decays to zero by the time $\tau \approx 7$.

1. Introduction

The experiments described in this paper arose out of work on unsteady flow in collapsible tubes. When a segment of collapsible tube is held open at both ends and subjected to an external pressure (causing collapse) while fluid is driven through it, self-excited oscillations are often observed (Conrad 1969). The cross-section of the tube, at a location near its downstream end, undergoes a large-amplitude oscillation between an approximately circular shape and a virtually flat, collapsed state. A simple lumped-parameter model of such oscillations (Pedley 1980; Bertram & Pedley 1982) indicates that the head loss associated with the separated jet emerging from

† Present address: Centre for Biomedical Engineering, University of New South Wales, P.O. Box 1, Kensington, Australia 2033.

the variable constriction is vital to the existence of the oscillations: they do not occur if there is no head loss. In our model we used the quasi-steady Borda–Carnot expression for the head loss, involving some pressure recovery (Batchelor 1967, §5.15), and oscillations were predicted. However, in both the theory and the experiments (Bertram 1982; Bonis 1979; Ur & Gordon 1970) the Strouhal number of the oscillations ($St = \omega d/\bar{u}_0$, where ω is the angular frequency, d the undisturbed tube diameter and $\bar{u}_0$ the mean velocity) is somewhat greater than one, which suggests that the fluid mechanics will not be quasi-steady. What we require from experiment, therefore, is an assessment of the difference between the quasi-steady head loss (or pressure recovery) and its actual unsteady value.

To this end we have designed an experiment to measure the pressure recovery in an approximately two-dimensional flow in a closed channel of rectangular cross-section (and undisturbed width a_0), one wall of which includes a time-varying indentation. First, however, we have performed a simpler experiment, examining impulsively started flow past a fixed indentation on one wall, and measuring as a function of time the reduction of head loss below its quasi-steady value during the separation process. In our experiments the Reynolds number ($Re = a_0\bar{u}_0/\nu$) lay in the range $300 \leqslant Re \leqslant 1800$. We chose a rather gently sloping indentation, with rounded convex corners (see figure 2 below), which approximates more closely to the longitudinal shape of a collapsible tube (at least of a thick-walled one) during oscillations than one with steep slopes and sharp corners. These features mean that separation develops gradually; its position depends on Reynolds number and does not depend on minute details of the flow near a sharp edge. Instead the foremost separation point moves slowly upstream before coming to rest at its eventual steady position on the smooth lee slope.

The development of separation in impulsively started flow over a smooth boundary in the presence of an adverse pressure gradient has recently received considerable attention, and a further aim of the present work is to shed some more experimental light on the subject. Previous experiments have been performed on either a circular cylinder (see e.g. Bouard & Coutanceau 1980) or an airfoil or similar shape (see e.g. Koromilas & Telionis 1980). The former were in a flow started impulsively from rest, while the latter have usually been in a flow changed impulsively from one steady state to another with a different adverse pressure gradient. There have also been many experiments in oscillating flow (e.g. McAlister & Carr 1979), including some in a constricted pipe (e.g. Young & Tsai 1973*b*). The latter, for example, noted that the head loss associated with separated flow was delayed relative to its quasi-steady value, but did not quantify the effect. Theory has been concentrated largely on the impulsively started circular cylinder: there have been numerical solutions of the full Navier-Stokes equations (e.g. Collins & Dennis 1973*b*), numerical solutions of the boundary-layer equations (e.g. Cebeci 1979) and analytical solutions based on the unsteady boundary-layer equations but extended to account for the modification of the outer flow at finite Reynolds number (Collins & Dennis 1973*a*; see also Proudman & Johnson 1962). There have also been one or two boundary-layer computations in other configurations (Walker 1978; Secomb 1979), but only the latter concerned an internal flow, examining the motion of a sudden indentation into an already developed steady channel flow.

Although differing in methods and in certain details, all these workers are broadly agreed on the sequence of events leading from the attached state to steady separated flow (see also Sears & Telionis 1975). After an impulsive start, there is an initial inviscid flow which is unidirectional but has associated with it an adverse pressure

gradient; the initial viscous response is the diffusion of a Rayleigh layer. After a certain time, the wall shear rate reverses at the point where $-\mathrm{d}U/\mathrm{d}S$ is maximum (U being free-stream velocity and S the distance along the boundary), e.g. the rear stagnation point of a circular cylinder, and the point of zero wall shear propagates rapidly upstream, leaving a thin region of reversed flow behind it. This reversal of wall shear, however, is not associated with a significant disturbance to the outer flow, boundary-layer theory can still be used to analyse it, and it should not be thought of as separation. Only subsequently, at a point downstream of the zero-shear point, does the boundary layer suddenly thicken, significantly modifying the outer flow, and often breaking away from the surface. It is this breakaway that in our view should be termed separation; afterwards boundary-layer theory is no longer applicable everywhere, whether or not the boundary-layer equations suffer a mathematical singularity at a finite time. The separation point also moves upstream, and eventually coalesces with the zero-shear point as the steady separated flow is set up.

There is no reason to expect different initial behaviour of the boundary layer in our case of channel flow. The initial flow will be irrotational, Rayleigh layers will develop on all boundaries, and wall-shear reversal will occur. It is only later that, with or without separation, vorticity will be present everywhere, and the assumption of an irrotational outer flow will become invalid; the eventual steady separated flow will of course be quite different from that in external flow. The steady case has been analysed by Smith (1976*a*, *b*, 1977), Smith & Duck (1980) and Smith & Daniels (1981) fo· different ranges of the governing dimensionless parameters. The version of the theory most applicable to the present steady flow experiments is outlined in §3.3 below, and its predictions of the pressure distribution and the position of separation are compared with the observations.

In the present paper we examine both steady and unsteady flow, by flow visualization and by measuring the pressure. Since unsteady flow visualization is always difficult to interpret, we have used three different techniques, the combination of which make us more confident in our interpretation than we otherwise could be. The experimental methods are described in §2. The results for steady flow, together with the theory already referred to, are given in §3, while the results for impulsively started flow are given in §4.

2. Experimental methods

The apparatus consists of a closed channel of rectangular cross-section along which aqueous fluids are impelled, with a return circuit consisting of rigid piping and a centrifugal pump (figure 1). A manually operated gate valve, normally left closed, can be partially opened when low channel flow rates are required. Impulsive flow starts are achieved by closing both gate valves, setting the pump running at the desired speed, and then opening the electrically operated gate valve in series with the channel. The arms of a U-tube mercury manometer are placed on either side of a constriction in the pipe, and the readings from it are used to determine steady flow-rate in the apparatus with reference to prior calibration against timed volume collections. One arm of the U-tube incorporates an orifice plate to prevent under-damped fluid oscillations when the flow is suddenly started. Fluid enters the channel via a baffle and a flow straightener to ensure a flat velocity profile at the channel entrance. The channel itself is 2.5 m long, with cross-section 100 mm high by 10 mm ($= a_0$) wide. To allow flow visualization, the top and bottom walls of the channel are of perspex; the side-walls are of aluminium. After 1.2 m of uniform channel the flow

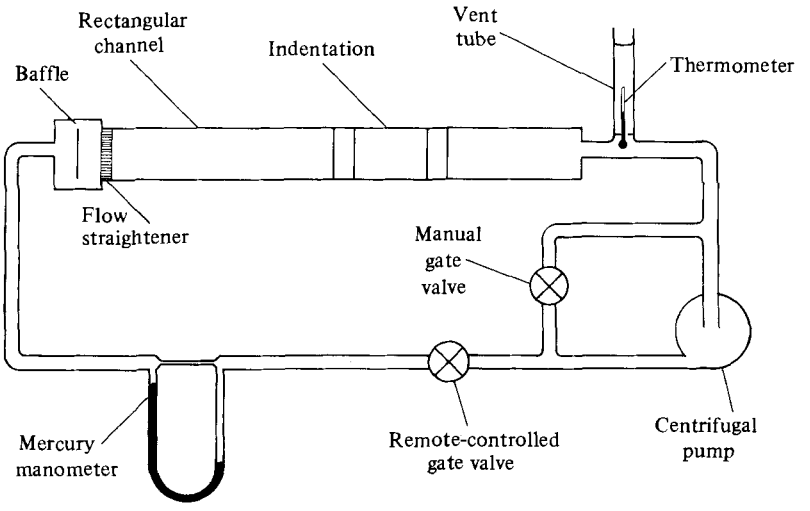

FIGURE 1. Schematic diagram (side view, not to scale) of the apparatus.

encounters an asymmetrical constriction consisting of a duralumin block of prismatic trapezoidal form attached to one sidewall and extending the full 100 mm channel height. This upstream length of channel was chosen to ensure that, in steady flow, the velocity profile across the 10 mm channel width should be fully developed (entrance length $= 0.04a_0 Re$; Schlichting 1968, p. 178). When the aspect ratio is 10, the fully developed flow near the centreplane is indistinguishable from two-dimensional Poiseuille flow, so it seems reasonable to assume that the entrance length is unchanged by three-dimensionality.

The channel width is linearly reduced to 5 mm over a longitudinal distance of 50 mm, and 100 mm further downstream is restored in similar manner to 10 mm (see figure 2). The convex corners of the indentation are rounded as shown in figure 2(*b*), where the shape on the midline of the downstream slope, $y = H(x')$, is plotted exactly (here x' is the longitudinal coordinate measured upstream from the downstream end of the indentation, and y is the transverse coordinate); the concave corners of the indentation are sharp. Opposite this indentation, perspex windows were incorporated in the side-wall. The only free fluid surface in the rig occurs in the vertical vent tube at the channel exit; access to this tube was restricted by an orifice plate to minimize fluid surging.

All our results pertain to flow in the horizontal plane halfway up the channel, 50 mm from each perspex wall. At this level the influence of the top and bottom boundaries is least, and by symmetry the flow over the indentation is expected to be qualitatively the same as in a genuinely two-dimensional channel (but not exactly; see §3.1). A series of pressure measurement ports, of internal diameter 0.84 mm, were incorporated in the wall and windows opposite the channel indentation, 5 mm above this midplane level in order that their shadows be clear of the midplane during flow visualization with transverse lighting. Flows were normally photographed with a camera mounted vertically above the channel at the downstream end of the indentation, looking downwards, with lighting via the bottom of the channel and/or the side windows.

The flow-visualization media used were polystyrene beads and liquid food colouring ('dye'). Blue food colouring was diluted with water and methanol in proportions giving a neutrally buoyant mixture in water at the same temperature. White

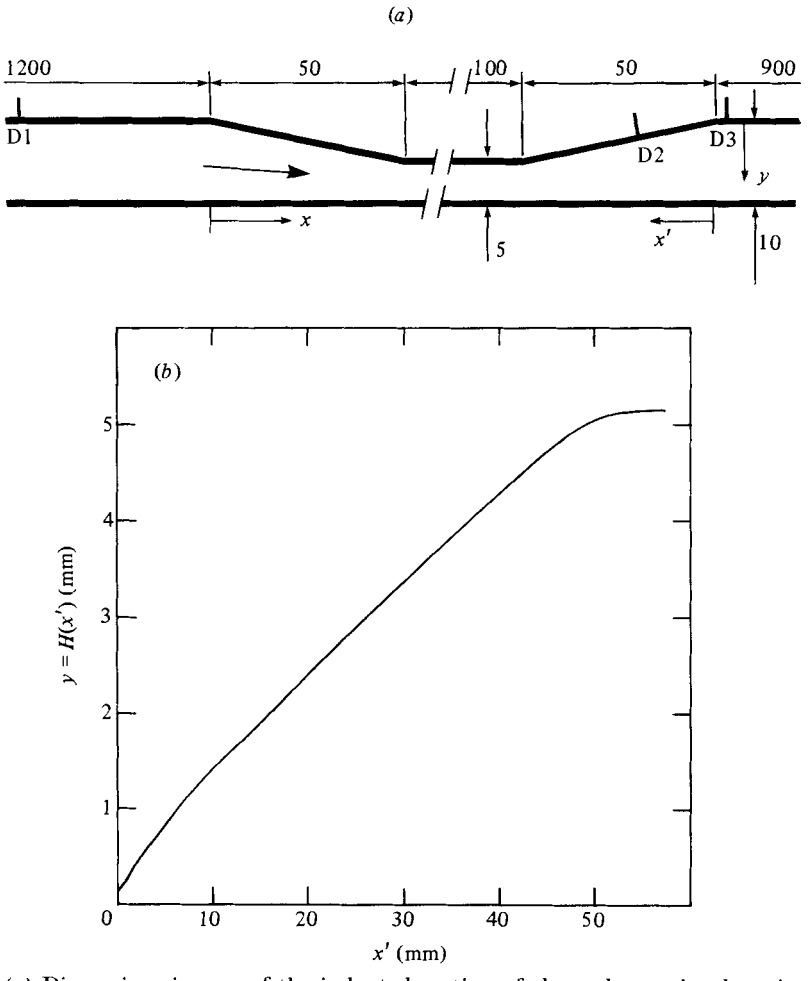

FIGURE 2. (*a*) Dimensions in mm of the indented section of channel, seen in plan view, showing the approximate locations of the midplane dye ports D1, D2, D3. Note that distance x is measured downstream from the start of the indentation, while x' is measured upstream from the end, and y is measured from the undisturbed position of the indented wall. (*b*) Detailed shape of the lee slope of the indentation on the midline, $y = H(x')$, with lateral dimension enlarged 10 times.

polystyrene beads (Shell Chemicals) were sieved into size grades up to 210 μm and used with mixtures of glycerol and water as the working fluid. Densities of about 1.04 times that of water were required for the beads to be neutrally buoyant on average, as determined by centifuging. Dye or bead–glycerol–water mixture was injected either via one of the pressure ports opposite the indentation, or via a port in the indented wall 71 mm before (D1) or 3 mm after (D3) the indentation, or via a port (D2) in the sloping lee of the indentation itself, 20 mm from the downstream end (see figure 2*a*). These three ports were located in the channel midplane of symmetry. For still photographs a Minolta SLR camera with 50 mm macro lens (viewing angle 47°) was employed; the ciné camera was a Bolex H16 loaded with Ilford Pan F operating at 64 frames/s, with either a zoom telephoto lens set at approximately 55 mm focal length and angle of view 8.5°, or a 10 mm Switar lens (angle of view 52°). Both the surface of the indentation and the plane wall opposite were scribed with vertical lines

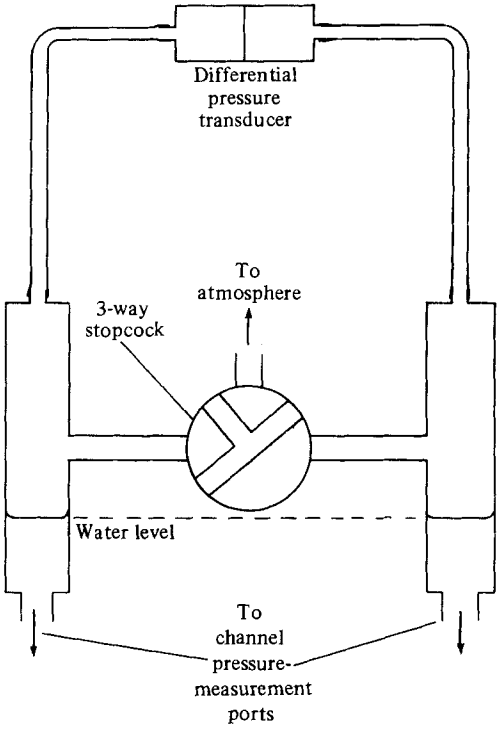

FIGURE 3. Schematic diagram of the steady-pressure measurement apparatus.

at 10 mm projected longitudinal spacing to allow quantitative measurements of marked fluid position when using a lens with wide angle of view. The telephoto lens was used exclusively with the beads, to reduce lighting halation from the walls. Lighting for these films was provided by a 1000 W Prinz IQ Movielite focused by a bicylindrical lens to shine through the side windows. Metal blinds defined a horizontal slit for the light beam at the channel midplane level, so that only those beads floating at the correct level were illuminated. Lighting for the dye photographs was provided by a 250 W slide projector, shining directly through the side windows and via a mirror and opalescent screen through the bottom channel perspex. The ciné films were subsequently analysed frame by frame by hand measurements of image positions, using an analytical projector to enlarge the negative image approximately fifty times.

For steady-flow pressure measurements a Gaeltec 8T transducer was used in the configuration shown in figure 3, which allows wet/wet differential pressure measurements with a dry transducer. Since the pressures to be measured are extremely small relative to atmosphere, the air columns behave almost as if incompressible. Were this strictly true (and the transducer volume displacement under differential pressure truly zero), then the water columns would not change height, and pressure changes at the ports would be transmitted without attenuation to the transducer. In practice, measurement of the water-column height with changing channel hydrostatic pressure showed that the attenuation caused by height changes amounted to 1.4 % of the true pressure difference at the channel. For impulsive-start measurements two Druck PDCR 10/L wet/dry differential transducers were employed, and the amplified outputs differenced digitally. When loaded with the working fluid, these transducers had a resonant frequency between 45 and 65 Hz (underdamped). A least-squares

system identification procedure (Åström & Eykhoff 1971) was implemented on a Computer Automation, Inc. minicomputer (LS1-2 processor and store, with Cambridge University Engineering Department in-house interfaces to I/O units) to determine the frequency response of each filled transducer. A digitally generated pseudorandom noise signal was amplified and used to drive an electromagnetic vibrator arranged to alter the volume of a closed air-filled chamber. The resulting pressure changes were sensed both by a dry reference transducer (Endevco 8507) and the transducer under test, which was plugged into an underwater port (identical to those in the channel) at the bottom of the chamber. Transients measured in the channel were later deconvolved using the inverse transfer function between the reference and the test transducer determined on the same day. For both steady and transient pressure measurement systems the primary static calibration was comparison with the reading of a Betz micromanometer (Instrumentenfabriek van Essen B.V.). Data from the Druck transducers were recorded digitally on flexible disc at a sample spacing of 5 ms. To avoid aliasing (introduction of a spurious signal frequency content below half the digitizing frequency, caused by the presence of frequencies above that limit in the original signal), the amplified transducer outputs were passed through 4-pole 90 Hz RC filters before digitizing.

3. Steady flow

3.1. *Flow visualization*

During steady flow with spatially averaged upstream velocity $\bar{u}_0$, the position of the separated eddy in the lee of the indentation was determined with the aid of dye injected continuously via port D1 or D3 (figure 2*a*). Figure 4 shows how the dye streak conveyed the location of the separation point as the upstream extremity of either the dye-free zone (figure 4*b*) or the recirculating dyed region (figure 4*a*). The location was found to be approximately the same for a given Reynolds number ($Re = a_0 \bar{u}_0/\nu$) whichever type of dye streak was used to assess it, as shown in figure 5, where it is plotted as a function of Re. Note that the length of the reverse-flow eddy shrinks to zero as Re is reduced to about 300. Separation did not occur at the beginning of the widening section of channel ($x/a_0 = 5$) because the convex corners of the indentation were rounded off (see figure 2*b*). Our experiments with dye injected through port D1 also show no signs of upstream separation for $Re \leqslant 2600$.

The location of reattachment of the boundary layer could not be accurately measured because flow in the lee of the indentation did not prove to be fully two-dimensional even at the halfway plane. In consequence, the dye streak that outlined the separated eddy did not reattach to the wall except at Reynolds numbers less than about 350, and in fact the recirculating dye tended eventually to spiral out of the midlevel plane and escape downstream. At Reynolds numbers above about 750 the free shear layer between the eddy and the core flow became unstable as shown in figure 4(*b*), and the resultant mixing caused the dye streak to disappear before reattachment.

Viewed horizontally through the side windows in the wall opposite the indentation, streaks emanating from dye introduced via port D1, and hence marking the flow outside the separated eddy, diverged from the midplane only slightly (for Re below that at which unsteadiness became apparent). However, the fluid velocities in the separated eddy itself are so small relative to those in the outer flow that minor three-dimensional effects can change the flow direction significantly. Figure 6 shows two examples in which dye is slowly injected via port D3. For Re up to and including

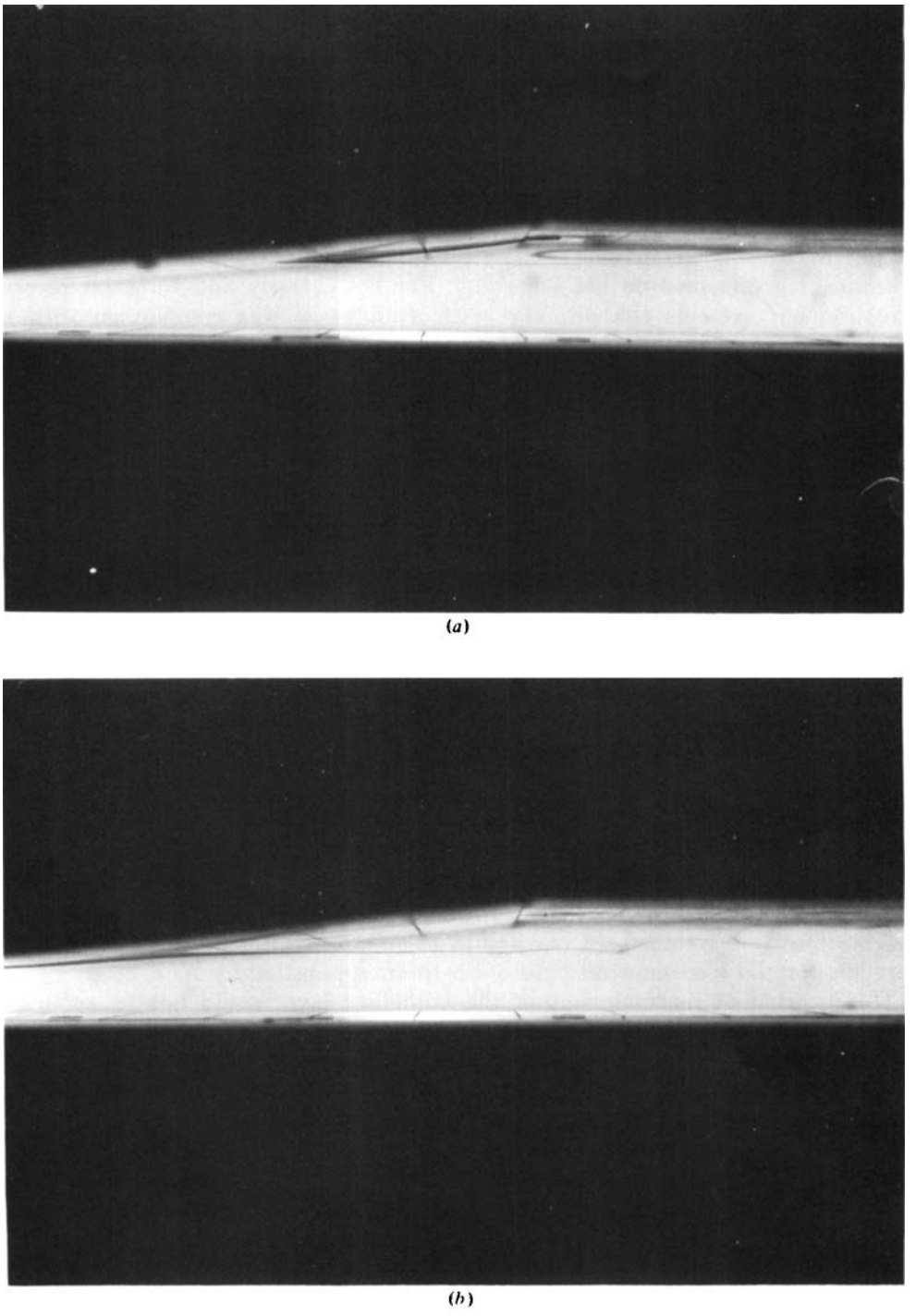

FIGURE 4. Steady-flow separation, viewed from above, with dye injected (*a*) via port D3 ($Re = 720$), (*b*) via port D1, illustrating the free shear-layer instability ($Re = 875$). In this and subsequent photographs there is a perspective to the view; the vertical lines scribed on both the lee slope of the indentation and on the plane wall enable the position of the wall to be seen. A reflection of the dye streak is visible in the polished surface on the lee slope; the position of the wall is halfway between the streak and its reflection.

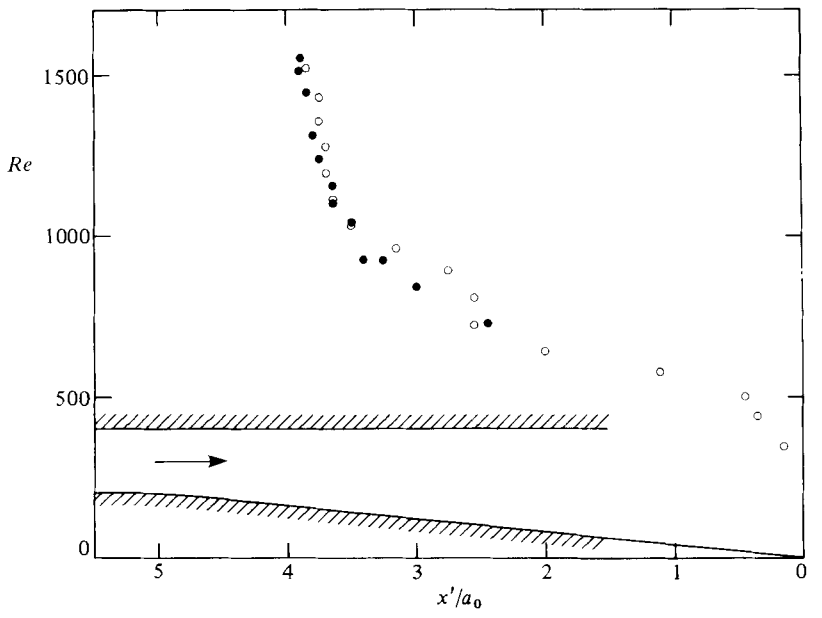

FIGURE 5. Location of the steady-flow separation as a function of Reynolds number, inferred from streaks of dye injected via port D1 (closed circles) and port D3 (open circles).

725 (figure 6*a*) the circulating dye rises from the midplane both as it moves upstream close to the wall and as it returns on the outside edge of the separation zone. When *Re* is further increased (to approximately 785), the dye moves downwards on its initial retrograde leg, then returns to the midplane and rises on its return. By $Re = 825$ this pattern gives way to descent from the midplane on both legs of its path (figure 6(*b*), $Re = 920$). With further increase in flow rate, the dye track becomes markedly unsteady, and by $Re = 1150$ the unsteadiness is such that the dye streak appears both above and below the midplane at different instants. Throughout this Reynolds-number range the dye ultimately spirals upwards close to the top of the channel, and there eddies in a faint imitation (because of dilution by mixing by this stage) of the separated recirculating flow close to the midplane. In the range where the dye initially descends, the subsequent route is gradual re-ascent to the midplane at the downstream end of the return leg and on the second retrograde leg, and then a steep ascent out of the area visible through the channel side windows, which extend 15 mm above and below the midplane. When the Reynolds number is sufficient for unsteadiness, the dye sometimes spirals downwards to the bottom of the channel instead. At $Re = 920$, where the unsteadiness is slight, the dye may escape the recirculation via the top of the channel for several seconds, then briefly switch to escape via the bottom with only marginal alteration in the downwards initial retrograde leg. At all Reynolds numbers where the dye track could be followed around the eddy at the top or the bottom of the channel, the separation point at this level appeared to be further upstream than that close to or on the midplane. This observation was confirmed when dye was injected via port D2, on the lee slope, and suggests that the separation line made up of the separation point at all vertical levels curves upstream away from the midplane. Such behaviour has also been observed by Young & Tsai (1973*a*) on asymmetrical obstructions in tubes; see also Cowley (1983) for a theoretical discussion.

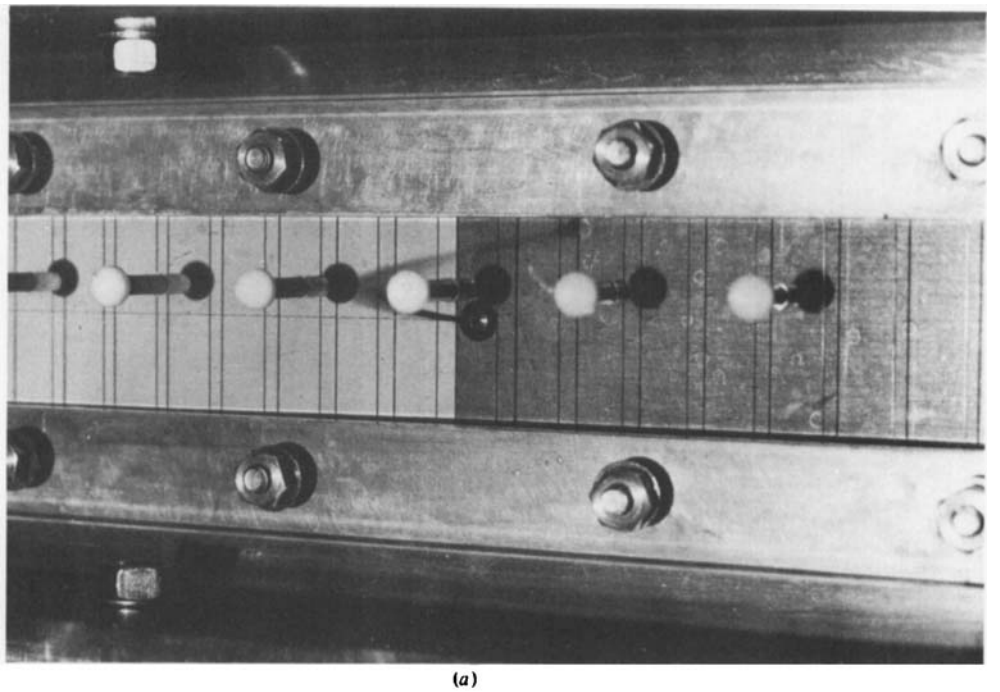

(a)

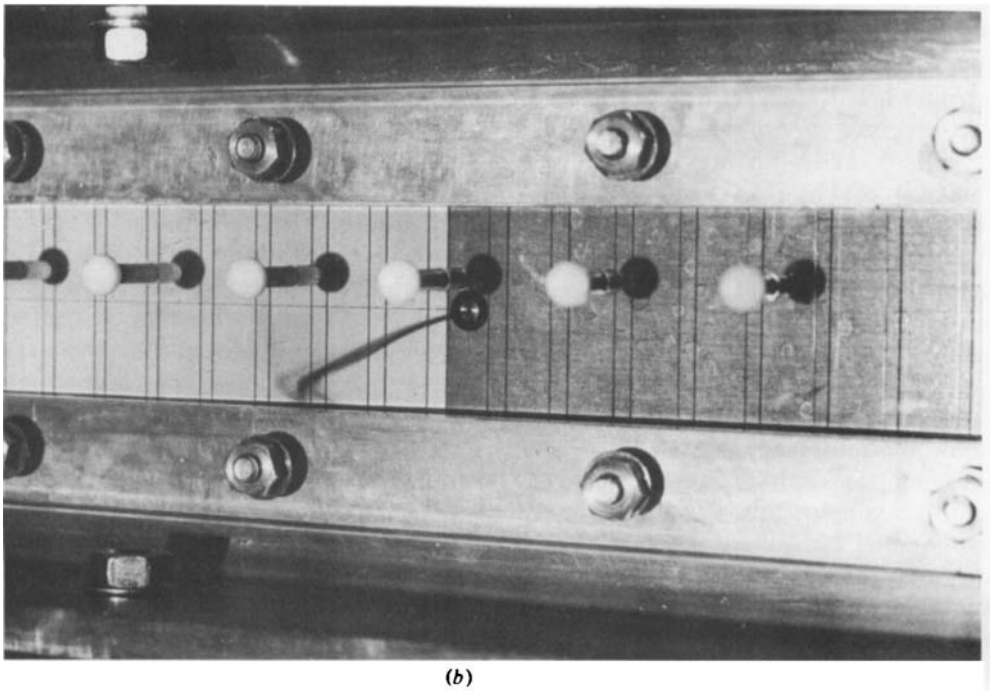

(b)

FIGURE 6. Side view of dye injected via port D3 in steady flow at (a) $Re = 725$, (b) $Re = 920$, showing how the flow in the separation bubble is not two-dimensional. (Port D3 is at the centre of the shiny circle surrounded by a dark ring in the middle of the photograph.) The main flow direction is from left to right; the dye streak at first moves upstream to the left.

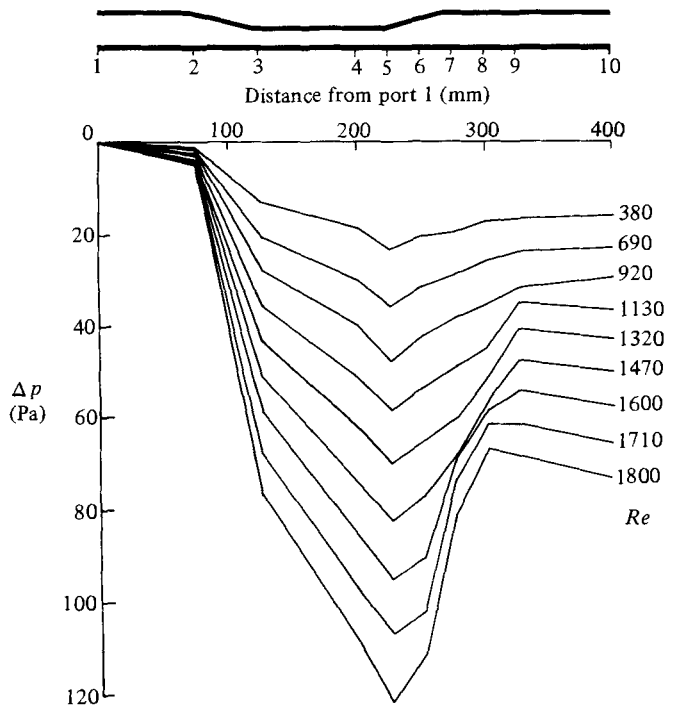

FIGURE 7. Steady-pressure measurements past the indentation at nine values of *Re*. The schematic diagram shows the pressure-port locations relative to the indentation.

The reason for the asymmetrical flow is not known. When this behaviour was first noticed, the channel was taken apart, carefully measured, and reassembled with accurately machined hardened steel dowels to guarantee that the channel width at each streamwise location is uniform from top to bottom, at least to the limit of attainable accuracy. This precaution did not alter the flow patterns. Neither was the dye rising owing to its own buoyancy; at zero flow rate the dye would fall extremely slowly (it being impossible to achieve absolutely neutral buoyancy, if only because of minute temperature differences). Even at the lower Reynolds numbers in the above range, vertical velocity of the dye in the recirculating fluid was so far in excess of the stationary sink rate as to make it plain that dye density effects were not responsible. It is conceivable, since no precautions were taken againt them, that there were sufficiently large temperature gradients in the rig to drive some sort of natural convection, but there would still be difficulty in explaining the change of sign of the vertical velocity as *Re* increased.

3.2. *Pressure measurements*

Figure 7 shows how the static pressure on the wall opposite the indentation varies with longitudinal position, for nine different steady flow rates. Each measurement was made with the steady differential pressure transducer connected between the furthest upstream port (no. 1) and one of the downstream ports, so that the value of the pressure drop Δp relative to the first port as baseline is given slightly more accurately than the pressure drop between any two adjacent downstream ports. The location of the ports is given by reference to the diagram of the indented part of the channel. Port 2 is here located 4 mm downstream of the start of the indentation

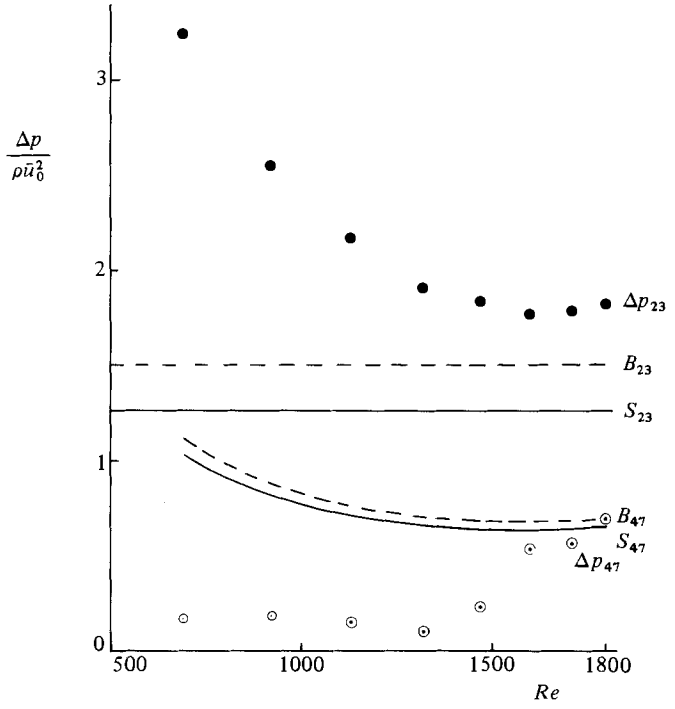

FIGURE 8. Dimensionless pressure difference, as a function of Re, between ports 2 and 3 (Δp_{23}, closed circles) and between ports 4 and 7 ($-\Delta p_{47}$, open circles). Broken lines (B_{23}, B_{47}) represent the crude theory of (1) and (2); full lines (S_{23}, S_{47}) represent the more rational theory of (6).

($x = 4$ mm), 75 mm downstream of port 1, but was subsequently (for unsteady measurements) relocated to a site 65 mm downstream of port 1, in the straight channel.

3.3. *Theory*

The crudest possible theory for steady flow in the geometry of figure 2 would neglect viscosity, would ignore the fact that the upstream velocity profile was not flat, would assume quasi-one-dimensional flow, and would use Bernoulli's theorem, coupled to the equation of conservation of mass, to infer the pressure everywhere. This would predict a pressure drop across the upstream slope of

$$\Delta p_{23} = 1.5\rho\bar{u}_0^2, \tag{1}$$

where Δp_{ij} is the pressure drop between ports i and j, since the maximum height of the indentation is exactly half the channel width. Such a theory could not predict separation, but, assuming the separation bubble to be parallel-sided, it would predict a pressure recovery on the downstream slope equal to the difference between the values of $\frac{1}{2}\rho\bar{u}^2$ in the narrowest section and at the separation point. Thus the theory would predict

$$\Delta p_{47} = -\tfrac{1}{2}\rho\bar{u}_0^2\left[4 - \frac{1}{(1-h_s)^2}\right], \tag{2}$$

where $a_0 h_s$ is the height of the indentation at separation.

The values of $\Delta p_{23}/\rho\bar{u}_0^2$ and $-\Delta p_{47}/\rho\bar{u}_0^2$ derived from the results of figure 7 are plotted against Re in figure 8 (closed and open circles respectively). The 'predictions'

(1) and (2) are shown as the broken lines B_{23} and B_{47}; the value of h_s required in (2) was estimated from figure 5. There is clearly a large discrepancy at lower Reynolds numbers, but it decreases rapidly as Re increases: at $Re = 1710$, for example, the discrepancy is only around 20% for each quantity. Moreover, in each case the discrepancy consists of an underestimate of pressure drop, as expected from the neglect of viscosity. The importance of viscosity can be further appreciated from the large pressure drop along the top of the indentation (Δp_{34} or Δp_{35}) revealed in figure 7.

The agreement with experiment could clearly be improved by merely superimposing a Poiseuille pressure gradient on to the predictions from Bernoulli's theorem, assuming quasi-unidirectional flow everywhere. However, the use of both Bernouilli's and Poiseuille's equations at the same values of Re is clearly inappropriate; a more rational theory must be sought. In recent years Smith and his colleagues have published a number of papers on high-Reynolds-number steady flow in an asymmetrically indented channel with Poiseuille flow upstream (Smith 1976*a*,*b*, 1977; Smith & Duck 1980; Smith & Daniels 1981), covering much of the geometrical-parameter range. The paper by Smith & Duck is on 'severe' constrictions and might seem to be the most appropriate to an indentation that occupies half of the channel width. However, it also requires relatively steep slopes to the indentation, and/or very large Reynolds numbers; the fact that it predicts separation from the upstream end of the narrowest part of the channel (the first convex corner, not somewhere down the lee slope), as well as upstream separation (not observed in our experiments) shows it not to be directly applicable, although all the relevant equations are contained in that paper. We here outline the appropriate large-Re theory for our experiment. It is based on the facts that the constriction is much longer than it is high but, in the large-Re limit, is much shorter than the lengthscale for viscous flow development, and that no upstream separation is observed. Except near the channel walls, therefore, the flow is governed by the *inviscid* boundary-layer equations; near the wall viscous boundary layers have to be interposed.

Formally, we let $a_0(\lambda X, y)$ be longitudinal and transverse coordinates, where $\lambda \gg 1$ is a parameter representing the longitudinal lengthscale of the indentation, so that $X = 0$ at the start of the indentation ($x = 0$, figure 2*a*) and $X = 1$ at the end ($x' = 0$). Take the boundaries of the channel to be at $y = \epsilon F(X)$ and $y = 1$, where $F(X) = 0$ for $X < 0$ and $X > 1$, $\max[F(X)] = 1$, and ϵ is a scale parameter equal to 0.5 in our experiments. Let $\bar{u}_0(u, v/\lambda)$ be the velocity components, where $\bar{u}_0$ is the average velocity in the upstream Poiseuille flow, given by

$$u = U_0(y) \equiv 6y(1-y),$$

and let $\rho\bar{u}_0^2 p$ be the pressure (in the Poiseuille flow $p = 12\lambda X/Re$). The Reynolds number $Re = a_0\bar{u}_0/\nu$ is taken to be large: $Re \gg \lambda \gg 1$. These variables are then substituted into the two-dimensional Navier–Stokes equations for incompressible fluids.

The present scaling, with $y = O(1)$, is expected to be appropriate to the flow in the core of the channel, outside the boundary layers near the walls, and, as expected, the viscous terms in the momentum equations are negligible, being $O(\lambda/Re)$ times the inertia terms. In this core, then, the equations reduce to the inviscid boundary-layer equations; the pressure $P(x)$ is independent of y from the y-component of the momentum equation. A first integral of these equations (Bernoulli's equation) shows that $P + \frac{1}{2}u^2$ is constant on streamlines, and, if we introduce the stream function ψ

such that $u = \psi_y$, we deduce that

$$\frac{\partial y}{\partial \psi} = \frac{1}{u} = [\bar{U}_0^2(\psi) - 2P(x)]^{-\frac{1}{2}}, \tag{3}$$

where $\bar{U}_0(\psi) = U_0(y)$ represents the upstream velocity profile. Integrating across the channel, we obtain

$$1 - \epsilon F(X) = \int_0^1 \frac{\mathrm{d}\psi}{[\bar{U}_0^2(\psi) - 2P(x)]^{\frac{1}{2}}} = \int_0^1 \frac{U_0(y)\,\mathrm{d}y}{[U_0^2(y) - 2P(x)]^{\frac{1}{2}}} \tag{4}$$

(Smith & Duck 1980, equation (4.3)). In the limit of small ϵ, this equation can be shown to reduce to

$$P(x) = -\tfrac{1}{2}\epsilon^2 F^2(X), \tag{5}$$

which is also the large-ϵ limit of the small-constriction problem, for which the displaced core is predicted to flow midway between the indented and the plane wall (Smith 1976*a*, *b*; Smith & Daniels 1981). In fact, when $\epsilon F = \frac{1}{2}$ (our maximum value), the two predictions (4) and (5) differ by only about 10%. Equation (4) relates the pressure at a given value of X to the displacement of the lower channel wall at that value. It will be valid as long as the equations for the viscous boundary layers at the wall have a solution and the boundary layers do not separate or become too thick. When the boundary layers have separated, the position of the separation streamline can be used in place of $\epsilon F(X)$, as long as X-rates of change do not become large.

The viscous wall layers have thickness $\delta = (\lambda/Re)^{\frac{1}{2}} \ll 1$ and, if the Prandtl transformation is used for the layer on the indented wall, can be shown to satisfy the classical boundary-layer equations for u and V, where $v = \epsilon F'(X)\,u + \delta V$ on the indented wall and $v = -\delta V$ on the plane wall. The pressure gradient in the x-momentum equation is $P'(x)$, and matching with the core flow is achieved by the condition that $u \sim [-2P(x)]^{\frac{1}{2}}$ as $Y \to \infty$, where Y is the relevant transverse coordinate. This problem does have a solution as long as $P'(X)$ remains negative or zero, but a Goldstein singularity will develop soon after P' becomes positive, leading to flow separation on the lee slope of the indentation, and on the flat wall opposite.

Equation (4) leads to definite predictions concerning the (measured) pressure drops Δp_{23} and Δp_{47}. Non-dimensionalizing as before (i.e. writing $\Delta p_{23} = \rho \bar{u}_0^2 \Delta P_{23}$ etc.), we obtain

$$\int_0^1 \frac{U_0(y)\,\mathrm{d}y}{[U_0^2(y) + 2\Delta P_{23}]^{\frac{1}{2}}} = \frac{1}{2}, \tag{6a}$$

$$\int_0^1 \frac{U_0(y)\,\mathrm{d}y}{[U_0^2(y) + 2\Delta P_{23} - 2\Delta P_{47}]^{\frac{1}{2}}} = 1 - h_s, \tag{6b}$$

where h_s is again the dimensionless height at separation, and we have assumed that the separation streamline remains appoximately parallel to the plane wall after separation (see figure 4; this is consistent with Smith & Duck's (1980) theory). These predictions are shown as solid curves S_{23} and S_{47} in figure 8, and it can be seen that they do not represent a significant improvement on (1) and (2): quite the reverse for the upstream pressure drop, in fact. The reason for the lack of agreement with experiment is presumably that viscosity still has no effect on the pressure drop since the limit $Re \to \infty$ has been taken. The advantage of the theory, however, is that it does represent the first step of a rational theory in which finite-Reynolds-number effects can be considered, at least on the upstream side of the indentation where there is no separation.

A further step that can be taken in the present theoretical framework is to integrate

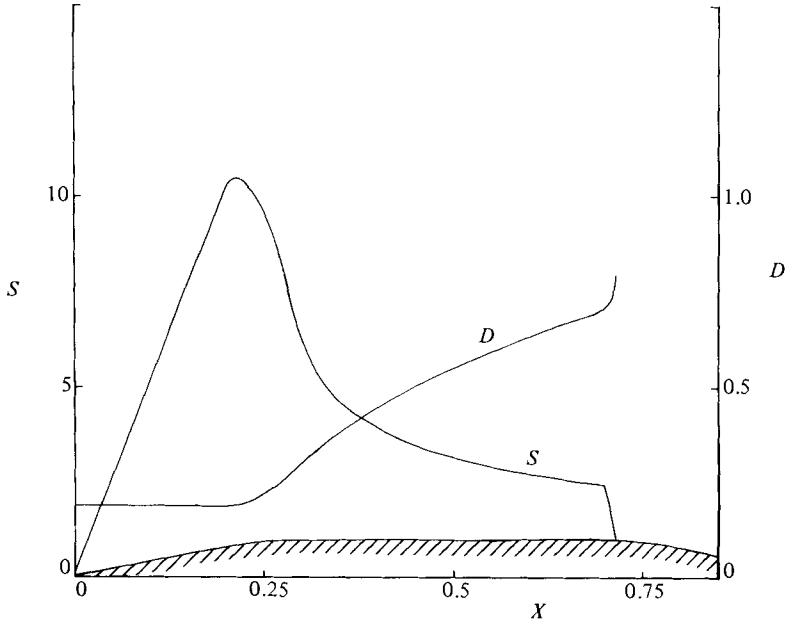

FIGURE 9. Predicted variation of dimensionless wall shear stress (S) and displacement thickness (D) with X.

the boundary-layer problem numerically, with the pressure distribution from (4) or (5), in order to predict the dimensionless wall shear, $S = U_y|_{y=0}$, the dimensionless displacement thickness D, and the point of downstream separation. This has been done for us (using (5) for the pressure) by Dr S. J. Cowley, for a geometry with rounded convex corners defined by

$$\begin{aligned} F(X) &= 4X \quad (0 < X < 0.25-b), \\ &= 1-\frac{1}{b}(0.25+b-X)^2 \quad (0.25-b < X < 0.25+b), \\ &= 1 \quad (0.25+b < X < 0.75-b), \\ &= 1-\frac{1}{b}(0.75-b-X)^2 \quad (0.75-b < X < 0.75+b), \\ &= 4(1-X) \quad (0.75+b < X < 1). \end{aligned} \tag{7}$$

The solution for $0 < X < 0.25-b$ is the similarity solution for stagnation-point flow:

$$u = 12Xf'(\eta) \quad \eta = 12^{\frac{1}{2}}\, Y,$$

where $f'(\eta)$ is tabulated by Schlichting (1968, p. 90). Thereafter Cowley used a boundary-layer integration programme based on that of Smith (1974). The results for $b = 0.05$ are shown as plots of S and D against X in figure 9. We see that S starts to fall rapidly, and D to rise rapidly, as soon as the flow encounters the rounded portion of the downstream corner at $X = 0.70$. By extrapolation (and breakdown of the boundary-layer integration routine) we predict the occurrence of a Goldstein singularity at $X \approx 0.72$. This is even earlier than when the corner is sharp ($X = 0.75$),

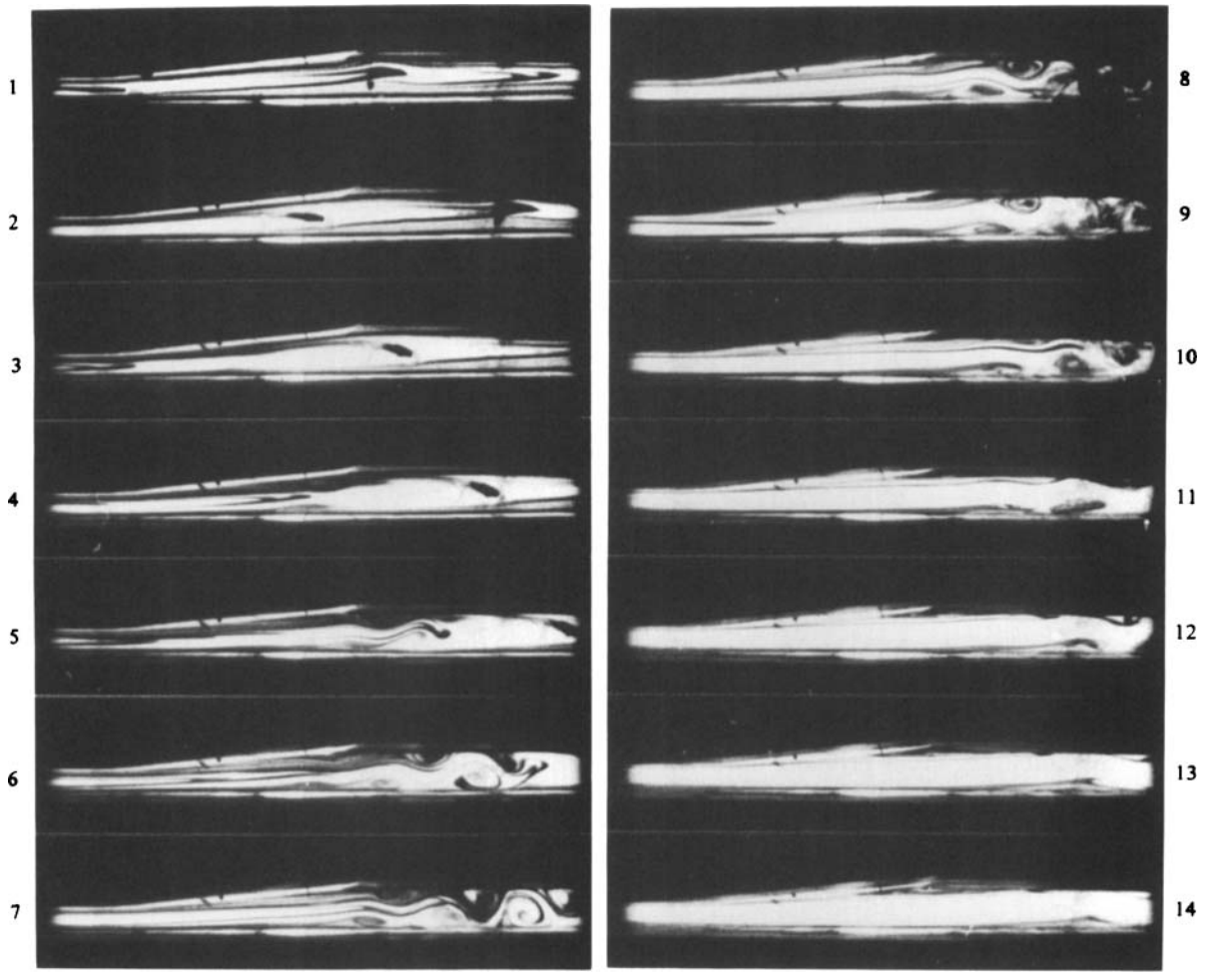

FIGURE 10. Sequence from ciné film with dye marking the whole flow ($Re = 800$). Panels 1–14 represent film frames 0, 16, 24, 32, 40, 48, 56, 64, 80, 96, 128, 160, 192 and 240 (at 64 s^{-1}) after the flow start. See caption to figure 4, for discussion of perspective view.

and emphasizes once again that the observation of the steady separation point some way down the lee slope is a finite-Reynolds-number effect, not yet incorporated in the theory.

4. Impulsively started flow

4.1. *Flow visualization*

Figure 10 shows a sequence of photographs taken from a ciné film during an impulsive flow start with final Reynolds number 800. For this event dye has been previously injected via port D1 with creeping flow, so that all the midplane fluid at rest opposite the indentation prior to the start is marked by dye in an arbitrary pattern. The behaviour depends on the final steady-flow Reynolds number: at the lowest Reynolds numbers of interest there is no separation and no instabilities are observed. With increasing Re (greater than about 300) separation occurs; moreover, instabilities are

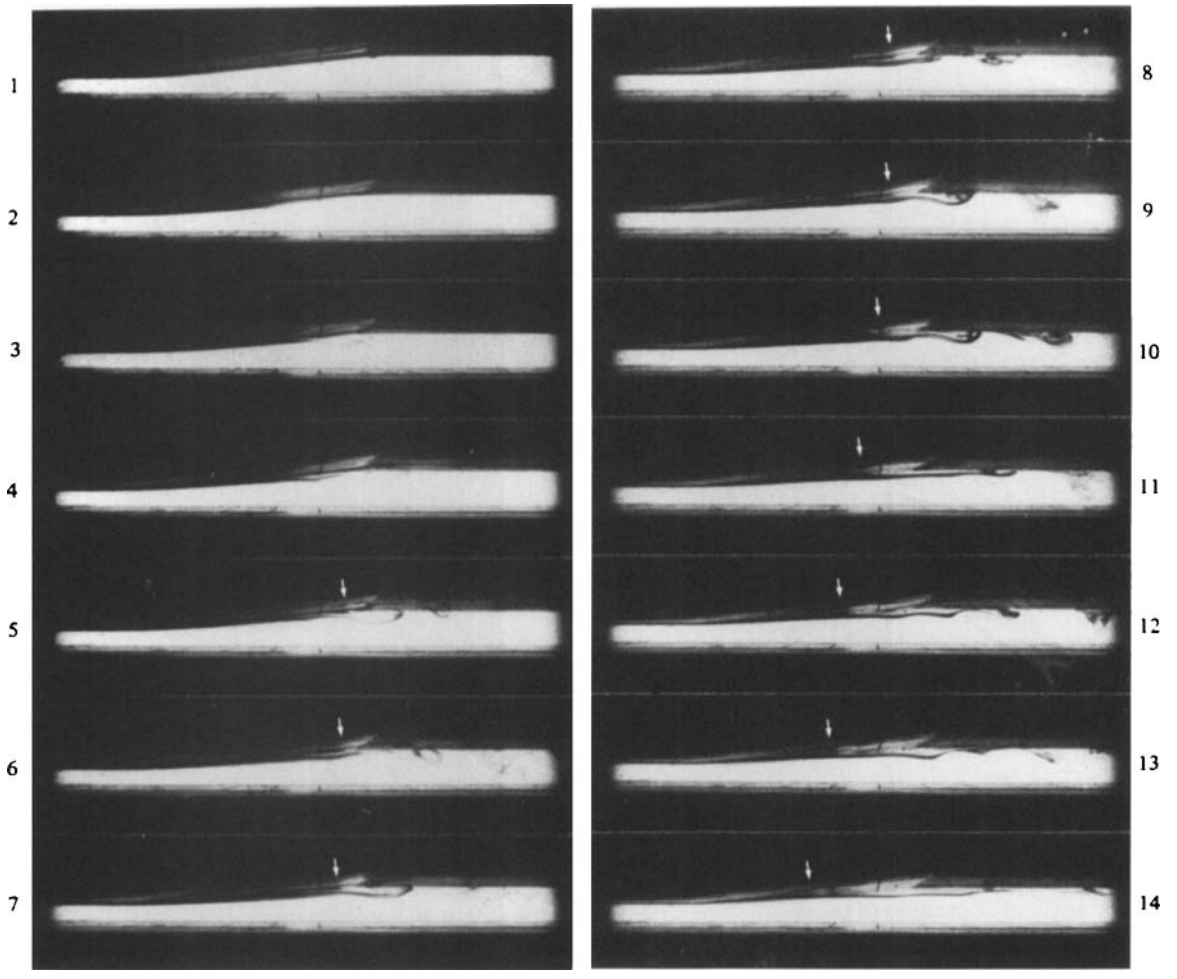

FIGURE 11. Sequence from ciné film with dye along the indented wall ($Re = 945$). Panels 1–14 represent film frames 0, 24, 32, 40, 48, 56, 64, 72, 80, 96, 128, 160, 192 and 256 (at 64 s^{-1}) after the flow start. Arrows show the location of the nose of the 'dye-free zone' (see text).

observed which may or may not be an intrinsic part of the separation process. For example, in panel 4 of figure 10(*a*), when dimensionless time, defined by $\tau = \bar{u}_0 t/a_0$, is about 4.4, vortices have developed on both the lee slope of the indentation and on the opposite wall. These eddies move downstream and interact in such a way that more vortices form alternately from either side, and the downstream flow has the appearance of a vortex 'street'. If the final Re is less than about 750, these vortices die away as the steady flow configuration is approached. At a final Re high enough for steady-flow instabilities, the ordered procession of vortices becomes irregular and further downstream gives way to turbulence. These vortices suggest that processes are at work which are similar to those associated with the quasi-steady instability of a velocity profile with an inflection point, as exists in this case.

After this initial flurry of activity, one observes the relatively slow retrograde progress of a zone of recirculating fluid originating at the downstream end of the indentation. It is this which eventually becomes the steady separated eddy. For closer

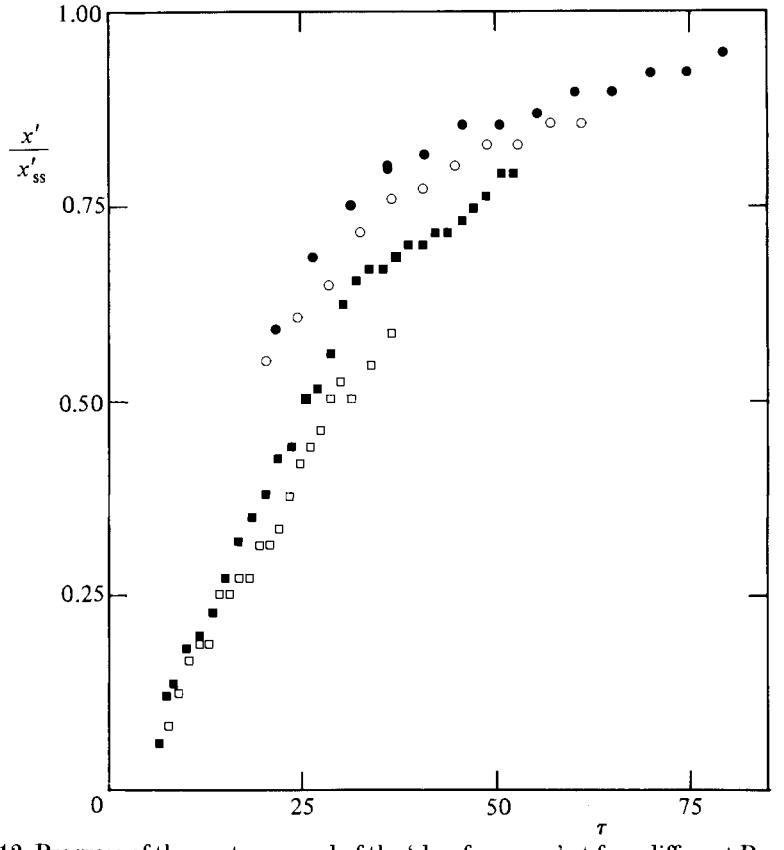

FIGURE 12. Progress of the upstream end of the 'dye-free zone' at four different Reynolds numbers. Vertical axis: longitudinal distance upstream of the end of the indentation, normalized by the equivalent distance of the steady-flow separation point at that Reynolds number. Horizontal axis: time, normalized by the convective timescale $a_0/\bar{u}_0$: □, $Re = 715$; ■, 945; ○, 1160; ●, 1380.

investigation of this process, dye was bled in via port D1 during creeping flow, before the impulsive start, so as to lie close to the indented wall all the way past the indentation. An example of the results is seen in figure 11. Usually, all the marked fluid moved parallel to the local wall initially after starting; then a streak originating close to the downstream convex corner of the indentation would emerge from the thickening dyed layer, on a course diverging from the sloping lee wall (panel 2; $\tau \approx 3.8$). As it proceeded downstream towards the end of the indentation, the lip of this stream became wavy (as for inflexion-point instability). This waviness was presumably responsible for introducing relatively dye-free fluid between the dyed fluid and the wall: opposite the end of the indentation, the streak rolled up as part of a largely dye-free vortex in the concave corner. Subsequently the dye-free zone became narrower and longer and slowly extended upstream (with some to-and-fro motion related to the unsteadiness near the concave corner), close to the sloping wall, as indicated by arrows in the sequence. Although the 'nose' of this retrogradely moving zone seemed to be approaching the appropriate steady-flow separation point, it became indistinct through mixing before reaching that location. Figure 12 shows the upstream progress of this nose for four different final Reynolds numbers. The four tracks only approximate to a common curve, when the axes are normalized as shown, because of the difficulty of identifying precisely the front of the recirculation zone.

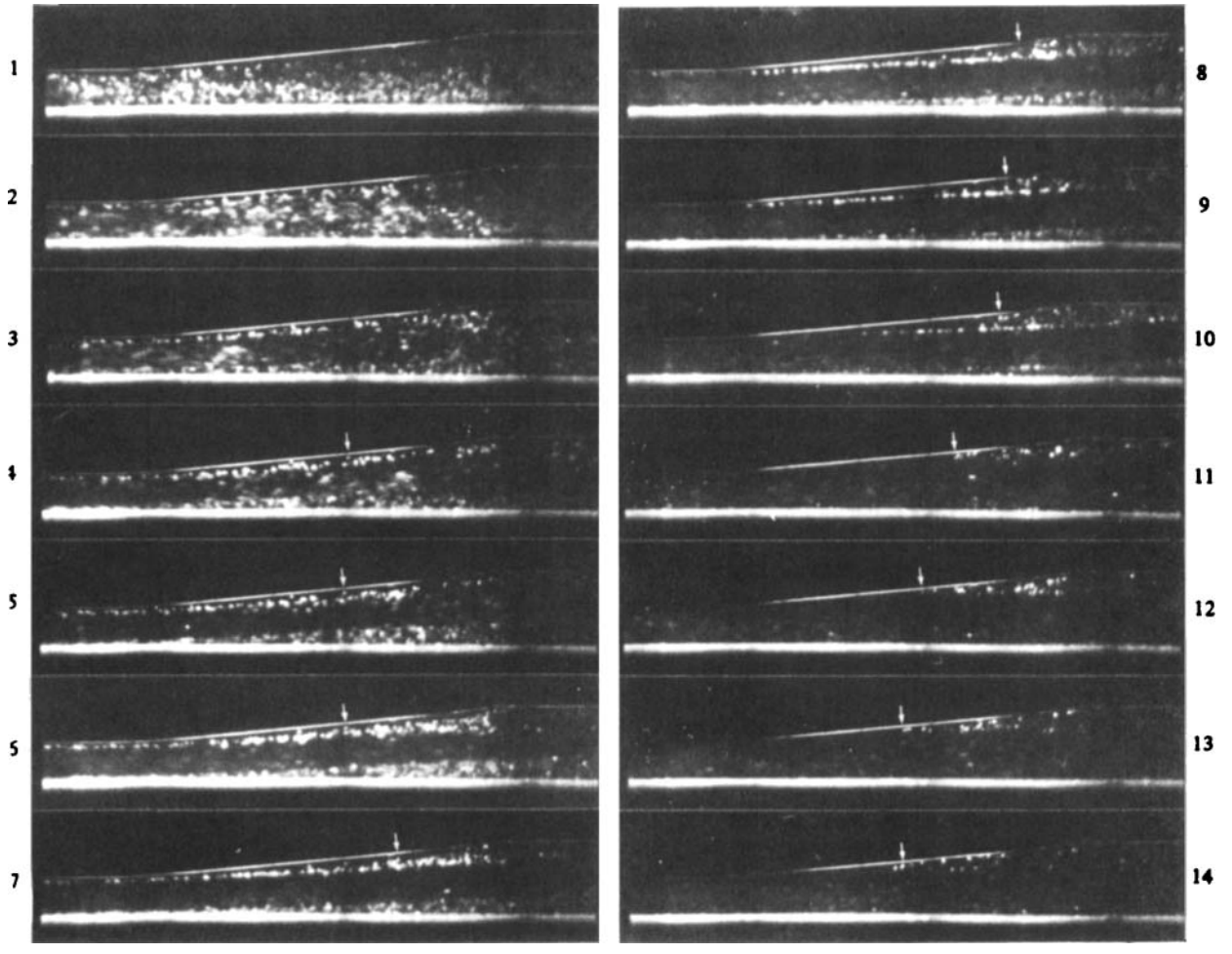

FIGURE 13. Sequence from ciné film with beads marking the whole flow ($Re = 955$). Panels 1–14 represent film frames 0, 8, 16, 20, 24, 32, 48, 64, 80, 96, 128, 160, 192 and 256 (at 64 s^{-1}) after the flow start. Arrows show the location of the furthest upstream retrogradely moving bead in the lee of the indentation at that instant.

To elucidate further the fluid behaviour in the lee of the indentation, a series of ciné films were taken using beads to mark the fluid as described in §2. Figure 13 shows a sequence of frames from one such (the beads appear larger than they in fact were, because of optical halation effects). For this event beads were introduced so as to be concentrated in the fluid next to the indentation. The rapidly moving flow in midstream therefore soon consists of relatively bead-free fluid forming a distinct track approximately midway between the indented and the straight wall with recirculation zones developing on either side. This is exactly as predicted for steady flow (and for high-frequency oscillatory flow) by Smith (1976*a*,*b*) as outlined above, However, later in the sequence the core flows more nearly parallel to the straight wall, so that the recirculating zone on the indented wall becomes wider at the expense of that opposite, the nose of which tends to move downstream. This is consistent with the theory if the separation streamline is taken as the upper edge of the channel (cf. Smith & Duck 1980).

Such ciné films were analysed frame by frame to determine the locations of upstream-moving beads as a function of time after the start. The arrows in figure 13 indicate the furthest upstream bead that was at that time moving upstream; the earliest to be seen (panel 4) occurred at $\tau \approx 3.3$. Such beads were always close to the wall, where flow reversal in response to an adverse pressure gradient is first expected. For a steady Reynolds number of approximately 950, figure 14 (*a*) shows the locations of retrogradely travelling beads close to the indented wall, while figure 14 (*b*) shows those close to the straight wall. Many experiments are combined here to produce sufficient information to allow the envelope of the reverse flow locations to be discerned. The envelopes indicate the earliest time after starting of reverse flow at a given location, and the furthest upstream location x'_{R} of reverse flow at a given time. In the case of the indented wall the area enclosed by this envelope all consists of reverse flow; for the non-indented wall it is not clear how far downstream the early reverse flow close to the wall extends. Figure 14 (*a*) indicates that the flow near the wall reverses approximately simultaneously over much of the lee slope, at $\tau \approx 4$, and that $x'_{\mathrm{R}}/a_0 \approx 2$ then. The subsequent decrease in x'_{R} was later shown to be an artifact associated with the use of finite-sized beads concentrated in one region of the channel; x'_{R}/a_0 in fact increased after the early appearance of reverse flow. Note, however, that x'_{R}/a_0 always remained less than 3.

Figure 14 shows that reverse flow first appears almost simultaneously on the two walls, at approximately the same location despite the asymmetry of the boundaries, as is predicted for steady flow by the theory. Subsequently, however, the sloping-wall reverse-flow point moves very slowly upstream, while that on the straight wall moves rather rapidly downstream, to a steady-flow location that could not be clearly defined, either from these experiments or from steady-flow dye injection, because straight wall separation in 'steady' flow only occurred definitely at very high Reynolds number, where the flow disturbances rendered the core flow unsteady. Figure 14 (*a*) also shows the location of the nose of the dye-free zone for the same Reynolds number, replotted from figure 12. Clearly reverse flow occurs upstream of and/or earlier than the recirculating eddy marked by the 'dye-free zone'. The rate of upstream movement of this zone in fact approximately corresponds to the retrograde velocity of fluid within the eddy, as was shown by comparing movements of individual beads with the progress of the nose of dye-free zones as in figure 14 (*a*).

To resolve this distinction between reverse flow and the separated eddy, a series of sudden starts was filmed with dye issuing continuously from port D2, on the lee slope 20 mm upstream from the end of the indentation ($x'/a_0 = 2$). One such event is shown in the sequence of figure 15. On starting, the cloud of dye already outside the port moves downstream with relatively little change in shape, while dye continuing to emerge extends in a line downstream of the port. When reverse flow begins at the port location (at frame 24, panel 3) this dye streak extends upstream as well. The reverse-flow zone is narrow, and, if dye enters the channel with finite velocity, its momentum may carry it across the zone, so that the dye now takes different paths to its eventual downstream destination. The sequence shown deliberately involves rather liberal use of dye to render the time of first reversal at the port obvious (see panels 3 and 4); in other films the dye feed rate was cut to the minimum possible commensurate with visibility of the streak. As the dye moves downstream to the end of the slope, it turns outwards away from the wall then curves back to its former course, executing a reverse curve that outlines an eddy wide enough to deflect the core flow significantly. The point at which the dye streak bends outwards

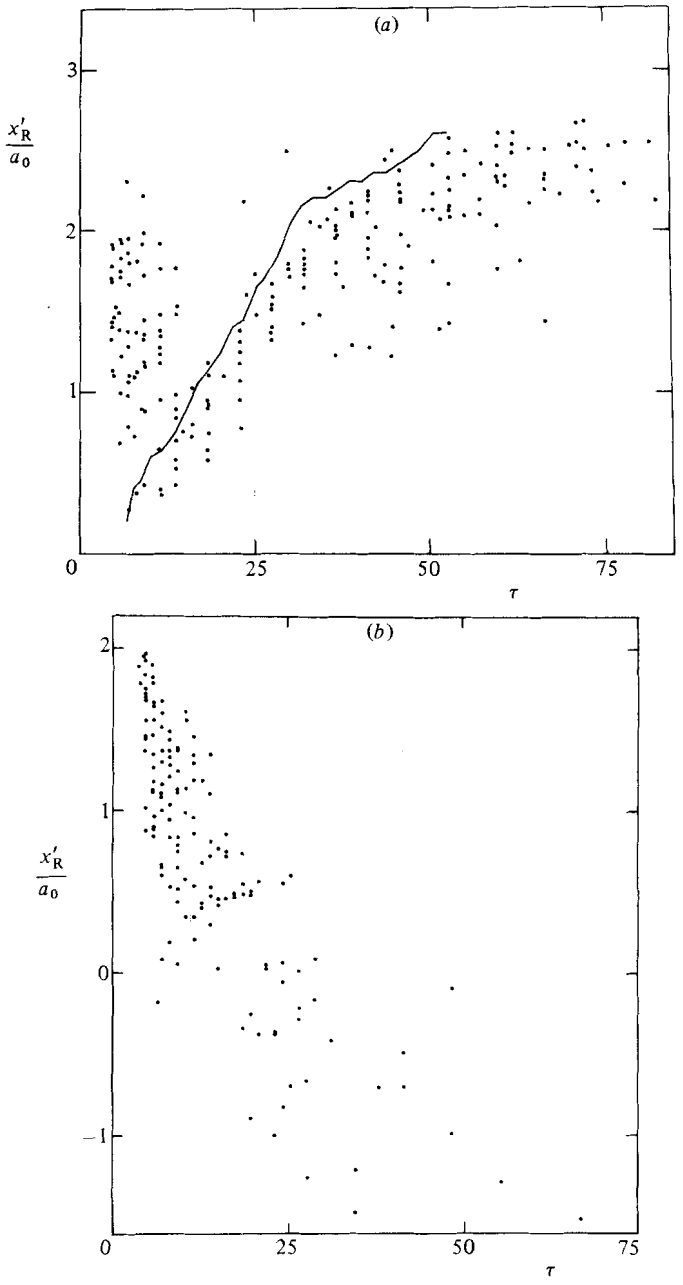

FIGURE 14. Dimensionless locations upstream of the end of the indentation, x'_R/a_0, of retrogradely moving beads *vs.* dimensionless time, $\tau = \bar{u}_0 t/a_0$, close to (*a*) the indented wall, (*b*) the non-indented wall ($Re = 950$). Also shown in (*a*) is the dye-free zone nose location for the same Re.

moves upstream with time steadily, except when surmounting the slope discontinuity at the downstream end of the indentation (see figure 2*b*). The position on the slope of this bend was too ill-defined for accurate comparison with the position of the nose of the dye-free zone described earlier, but there was approximate correspondence between them. Furthermore, the value of τ at which the bend passed the dye port

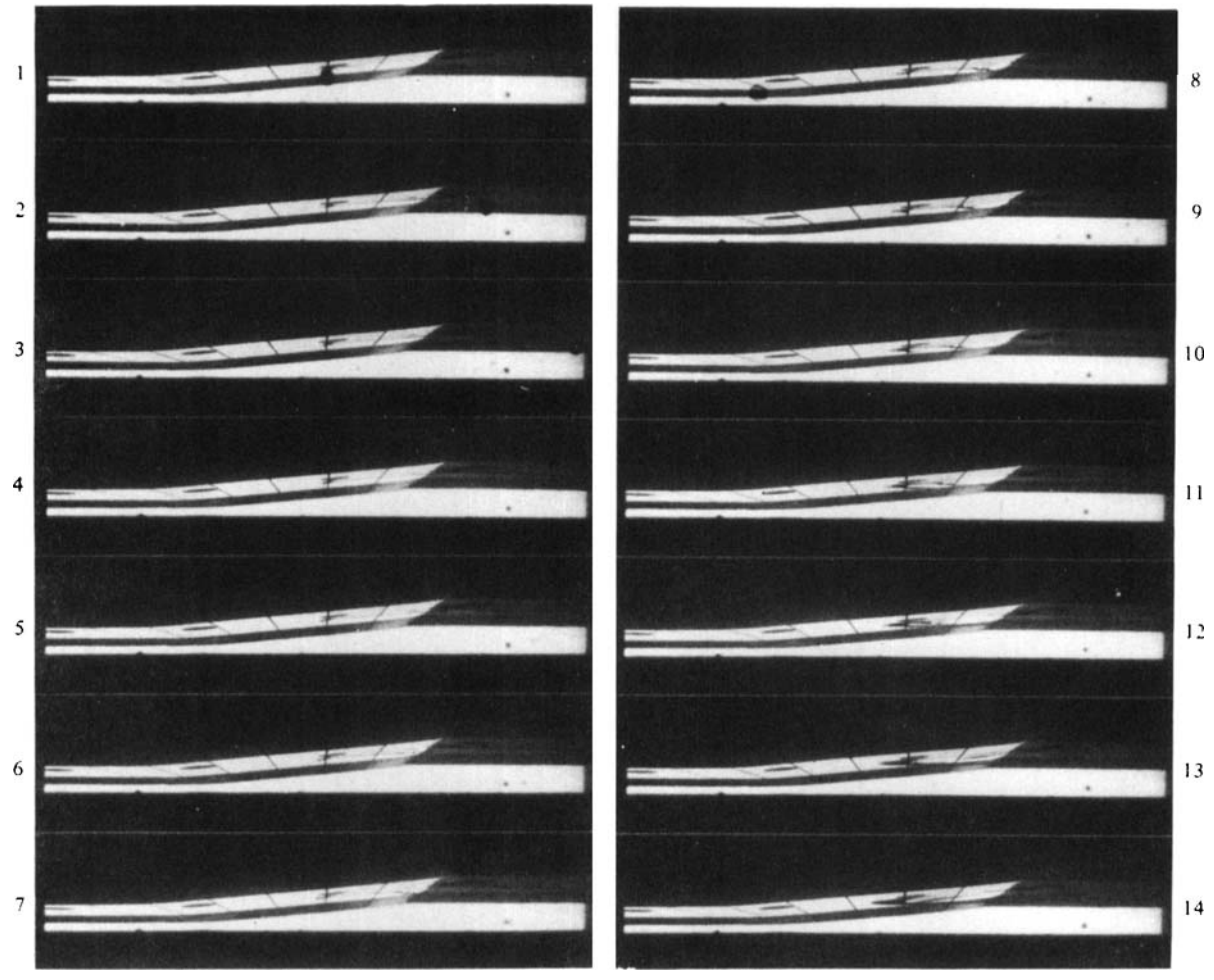

FIGURE 15. Sequence from ciné film with dye issuing from the sloping-wall port D2 ($Re = 980$). Panels 1–14 represent film frames 0, 16, 24, 28, 32, 36, 40, 48, 64, 80, 96, 128, 192 and 256 (at 64 s^{-1}) after the flow start. The dye port is situated halfway down the sloping wall, on the scribed line, which points towards the camera in this perspective.

agreed closely with the time at which the front of the dye-free zone reached $x'/a_0 = 2$ (figures 5 and 12). Figure 16(a) shows how the time of first reverse flow at $x'/a_0 = 2$ varies with final Re. Reverse flow occurs quicker at high flow rates, but, after normalization by the convective time $a_0/\bar{u}_0$, the time between the start of flow and reversal at this site increases slightly with Re. The same is true of the (rather later) time at which the outward bend in the downstream dye streak first appears on the slope ($x' = 0$), as shown in figure 16(b).

An important observation from figure 15 is the *absence* of vigorous eddies marked by this dye streak, until the eddy that starts at the downstream end has developed significantly (panel 6, for example). This is in contrast with figures 10 and 11, where the dye originated in the core, and reinforces the view that the vortices observed there were manifestations not of boundary-layer separation but of shear-flow instability.

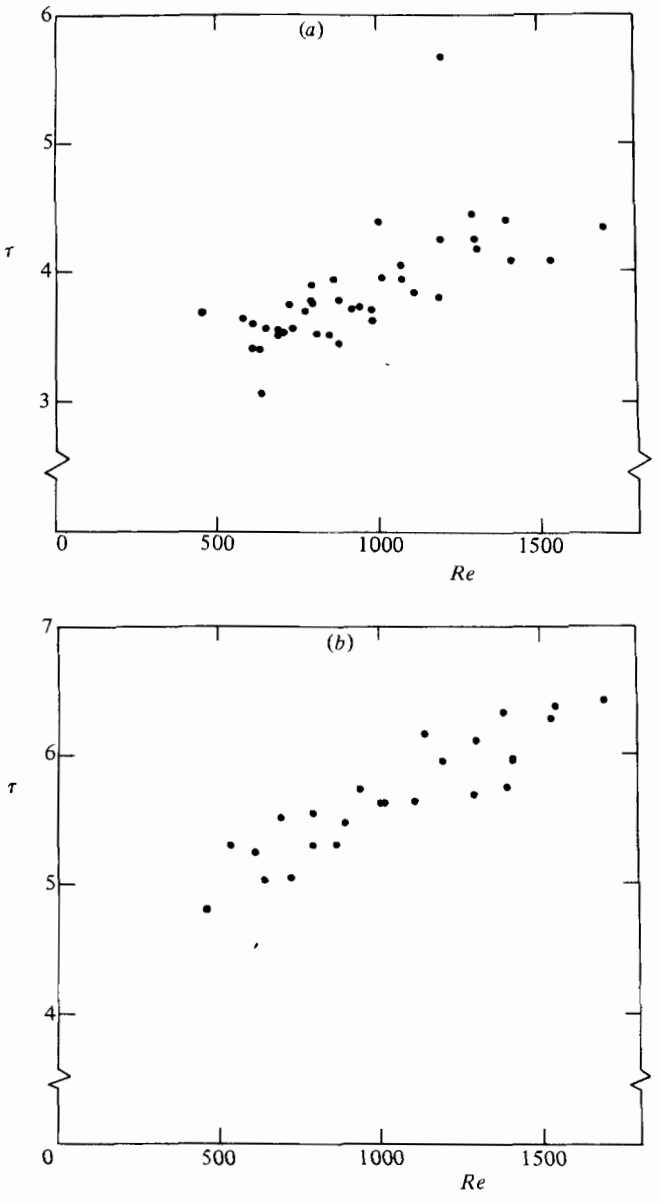

FIGURE 16. (*a*) Dimensionless time $\tau = \bar{u}_0 t/a_0$ of first reversal at port D2 *vs.* Reynolds number. (*b*) Dimensionless time τ of first arrival of the wide recirculating eddy on the indentation slope *vs.* Reynolds number.

4.2. *Pressure measurements*

The aim of measuring the unsteady pressure drop $\Delta p(t)$ between two ports spanning the lee side of the indentation (e.g. nos. 4 and 7 on figure 7) is to detect the gradual development of flow separation and to assess the departure of Δp from the value it would take if the separated flow patterns were quasi-steady. Thus we seek $\Delta p - \Delta p_{\text{pred}}$, where Δp_{pred} is equal to the purely quasi-steady pressure drop Δp_{qs} plus an unsteady contribution from the local fluid acceleration:

$$\Delta p_{\text{pred}} = \Delta p_{\text{qs}} + \Delta p_{\text{acc}}. \tag{8}$$

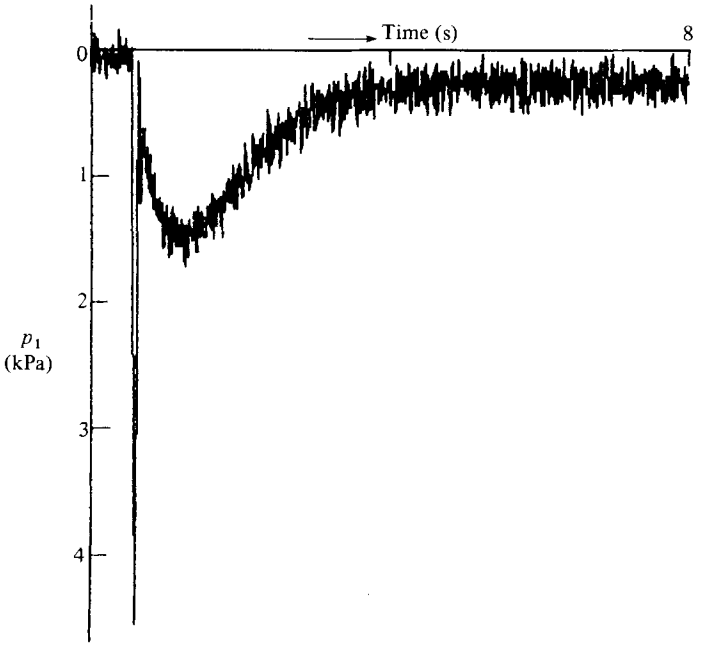

FIGURE 17. Variation of hydrostatic pressure at port 1 during an impulsive flow start ($Re = 1655$). Pressure increases downwards. Uncompensated for transducer frequency response.

If we know the spatially averaged velocity $\bar{u}_0(t)$ in the straight part of the channel then Δp_{qs} can be deduced directly from steady-state results such as those of figure 7. This term will incorporate a viscous pressure *loss*, associated with the (steady) separated flow, and an inertial pressure *recovery* due to the deceleration of the flow as it passes through the channel expansion (Bernoulli effect).

The accelerative contribution Δp_{acc} is obtained by integrating the unsteady inertia term between the two ports. We assume that the viscous boundary layer (Rayleigh layer) is at first very thin, and that the channel width varies sufficiently slowly for both the pressure p and the longitudinal velocity $\bar{u}$ to be inependent of the transverse coordinate and for the transverse component of velocity to be negligible. If $\bar{u}(x,t)$ is the spatially averaged longitiudinal velocity, we then have

$$\Delta p_{acc} = \int -\rho \frac{\partial \bar{u}}{\partial t}(x,t)\,\mathrm{d}x, \tag{9}$$

where the limits of integration are the x-coordinates of the two pressure ports and ρ is the fluid density. The same assumption gives

$$\bar{u}(x,t) = \frac{a_0}{a(x)}\bar{u}_0(t), \tag{10}$$

where $a(x)$ is the channel width at location x.

Thus all that is necessary to make the required correction to Δp_{qs} is to measure $\bar{u}_0(t)$, which we assume to be approximately equal to $u_0(t)$, the centreline velocity in the upstream straight segment of channel immediately after the flow start. The steady centreline velocity just upstream of the indentation was obtained from Pitot-static differential pressure measurements between a specially bored static port in the channel wall and a pitot tube of 1.3 mm outer diameter located with its open end

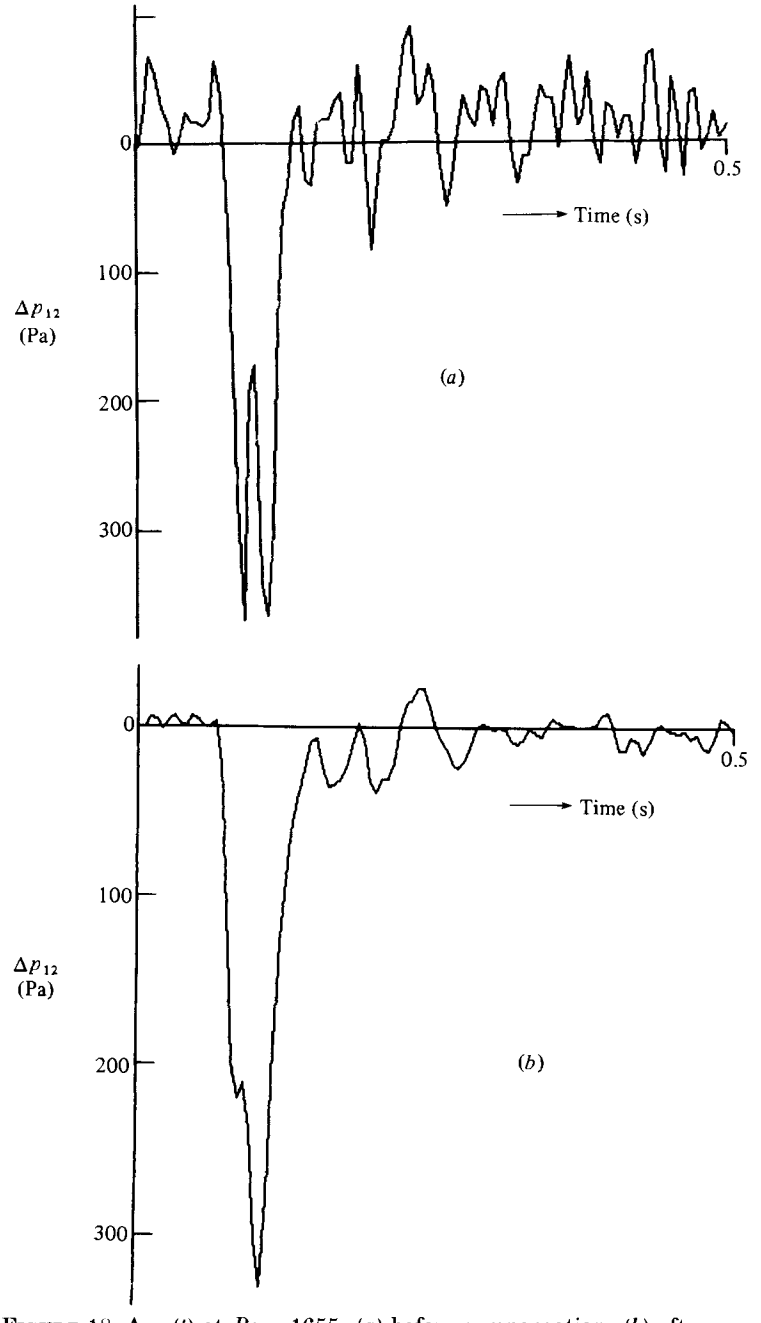

FIGURE 18. $\Delta p_{12}(t)$ at $Re = 1655$: (*a*) before compensation; (*b*) after compensation and averaging of ten events.

7 mm downstream of the static port. However, the unsteady centreline velocity could not be measured directly with the available instrumentation. The required velocities were therefore inferred from the results of pressure measurements between ports 1 and 2 in the parallel-sided channel, neglecting viscosity, as follows:

$$-\rho \frac{\partial u_0}{\partial t}(t) = \frac{\partial p_0}{\partial x}(t) \approx \frac{\Delta p_{12}(t)}{\Delta x_{12}}. \tag{11}$$

Figure 17 shows how the pressure at port 1 varied during an impulsive flow start, while figure 18(*a*) shows the 'raw' recorded $\Delta p_{12}(t)$, on a different timescale. The constriction in the vent tube entrance is responsible for the slow component of pressure change in figure 17, which does not contribute to the fluid acceleration. Compensation for transducer frequency response still left marked fluctuations in Δp_{12} at frequencies higher than that of the main fluid acceleration transient. These fluctuations are caused by imperfectly steady rotation of the centrifugal pump. Since they are not coherent with the flow start their influence can be reduced by averaging similar impulsive starts, and figure 18(*b*) shows how the noise was reduced after digital averaging of ten events, using the time of switching power to the remote-controlled gate valve as a synchronizing reference. Figure 19 shows the results of time integration of such averaged pressure differences to obtain the spatially averaged velocity of flow in the unconstricted channel at six different final Reynolds numbers. Also shown are the pitot-statically measured centreline velocities at the corresponding steady bulk flow rates. Since (11) assumes an inviscid fluid, the small component of $\Delta p_{12}(t)$ representing the early stages of boundary-layer growth (viscous resistance) is wrongly interpreted as accelerating the fluid, and the traces accordingly continue upwards after the genuine initial acceleration. For the remaining computations, $u_0(t)$ was therefore replaced by the corresponding measured steady centreline velocity when the derived value exceeded that.

In the comparison of Δp_{pred} with measured values of Δp, the chosen pair of pressure ports were no. 4, on the indentation 20 mm upstream of the start of the lee slope, and no. 7, 5 mm downstream of the end of the lee slope and 75 mm downstream of port 4 (see figure 7). The prediction for the accelerative component of $\Delta p_{47}(t)$ was calculated from (9)–(11) as

$$\Delta p_{47}(t)_{\text{acc}} = \frac{a_0}{\Delta x_{12}} \int_{x_4}^{x_7} \frac{\mathrm{d}x}{a(x)} \Delta p_{12}(t). \tag{12}$$

To obtain the best possible accuracy, $\Delta p_{47\text{qs}}$ was measured directly in steady flow, rather than by subtracting two of the measurements used in figure 7, and since port 2 had been moved (see §3.2), $\Delta p_{12\text{qs}}$ was also remeasured. Δp_{12} proved to depend linearly on $\bar{u}_0$, with a slope for the pressure gradient of 146 Pa s m^{-2}. This is in approximate agreement with the figure obtained by calculation from the final slopes (beyond 3 s) of the curves in figure 19, indicating that the accuracy of the unsteady pressure measurement system was sufficient for detection of pressure differences as small as 1 Pa between ports 1 and 2.

Figure 20 shows an example ($Re = 1655$) of the comparison between the measured $\Delta p_{47}(t)$ and the predicted $\Delta p_{47}(t)_{\text{pred}}$. As expected if separation is delayed and the inviscid flow initially occupies the whole width of the diverging channel, the measured $\Delta p_{47}(t)$ shows a greater pressure recovery than the prediction in the 0.4 s after the large accelerative transient. The time-course of the discrepancy in one case ($Re = 1655$) is shown in figure 21. This trace involves differences between differences between measurements, and the signal-to-noise ratio is accordingly low. In order to discern the underlying trends, we averaged out the fluctuations by taking the time-average of the trace over each $\frac{1}{8}$ s (25 samples). The results, normalized by the ultimate steady kinetic head $\rho \bar{u}_0^2$, are plotted against dimensionless time τ, for six different Reynolds numbers, in figure 22. It can be seen that the data coalesce to give a single characteristic time-course for the unsteady effects of interest. The discrepancy between measured and quasi-steadily predicted pressure drops has disappeared by $\tau \approx 7$.

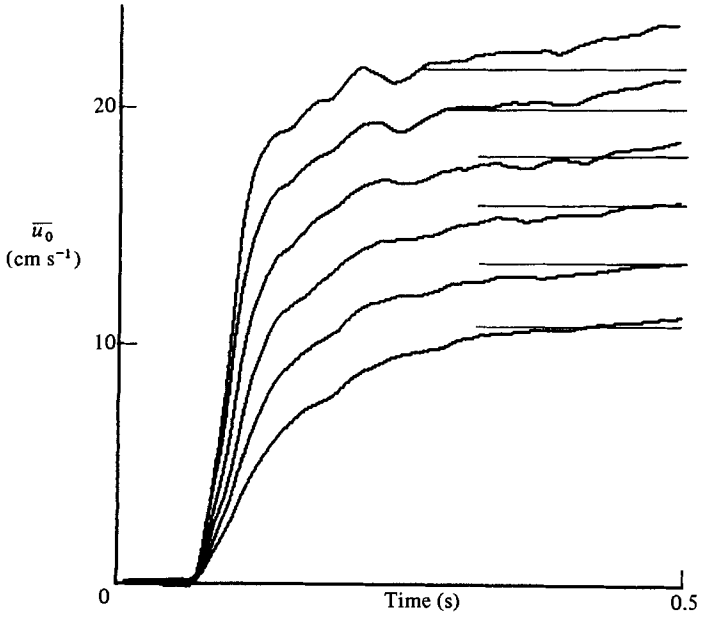

FIGURE 19. Computed $\bar{u}_0(t)$ at $Re = 675$, 860, 1055, 1245, 1455 and 1655. Also shown are the corresponding steady centreline velocities measured pitot-statically.

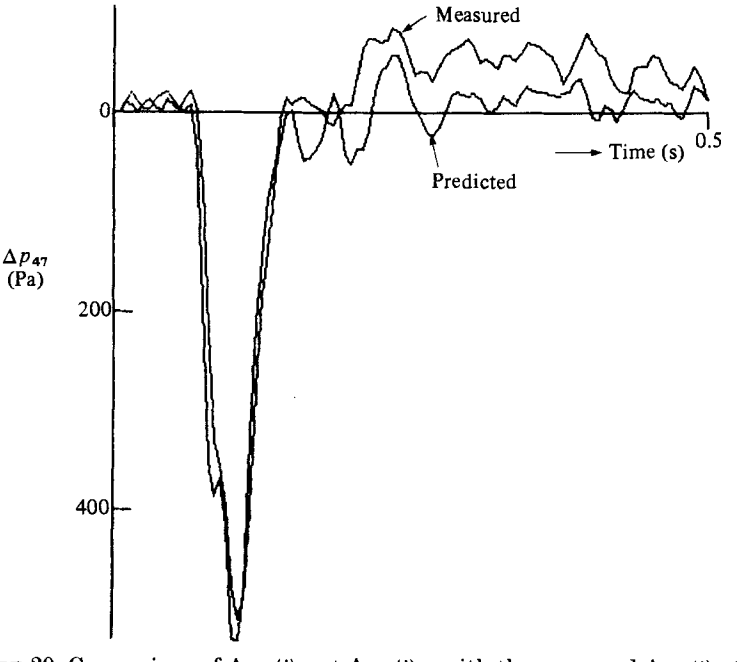

FIGURE 20. Comparison of $\Delta p_{47}(t)_{\mathrm{acc}} + \Delta p_{47}(t)_{\mathrm{qs}}$ with the measured $\Delta p_{47}(t)$ at $Re = 1655$.

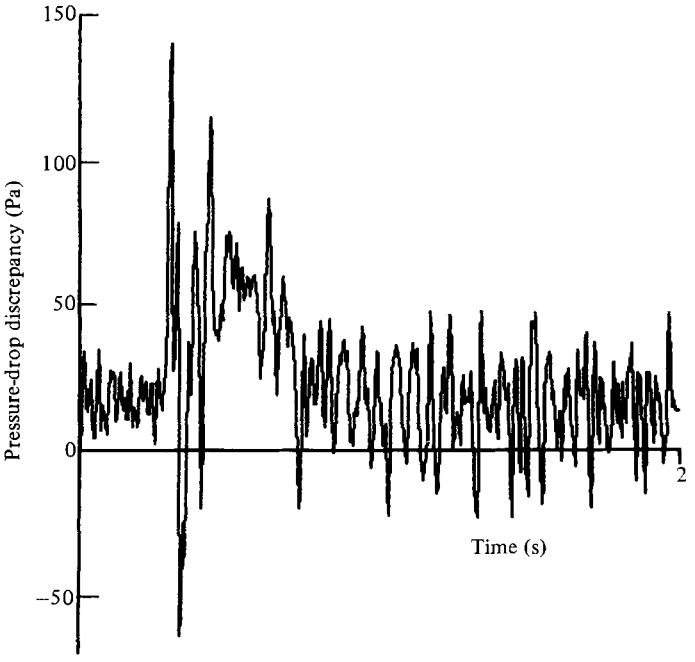

FIGURE 21. The difference between the measured and the computed pressure drops in figure 20.

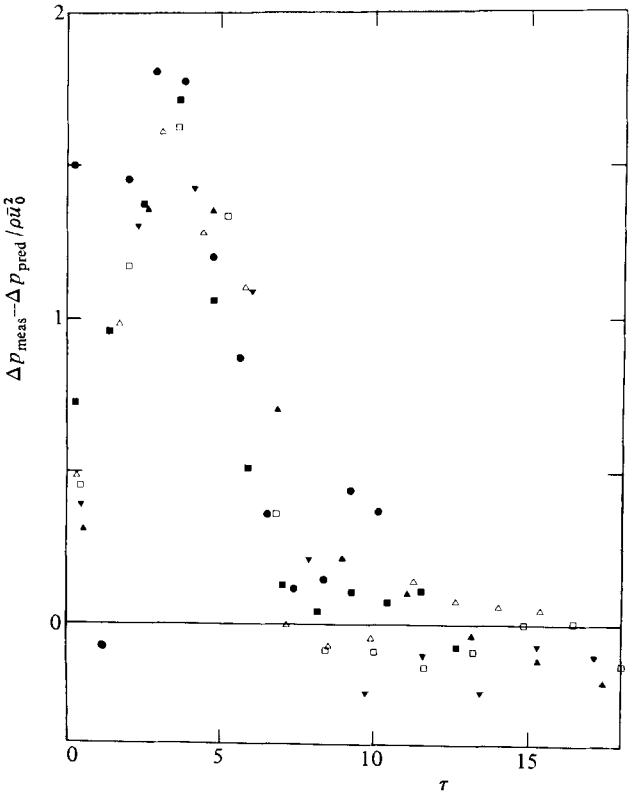

FIGURE 22. Difference between computed and measured pressure after time averaging in bins of $\frac{1}{8}$ s, for all six values of Re in figure 18, plotted with dimensionless axes: ●, $Re = 675$; ■, 860; △, 1055; □, 1245; ▼, 1455; ▲, 1655.

4.3. *Discussion*

If our only flow-visualization technique had been to bleed dye in through port D2 on the lee slope of the indentation (figure 15), then our qualitative description of how separation develops would have been the same as that outlined in §1. That is, a thin region of flow reversal develops on the lee slope at τ in the range 3.5–4.3 (figure 16*a*); a little later ($5.0 < \tau < 6.3$: figure 16*b*) a small but not narrow region of recirculating fluid develops at the concave corner at the downstream end of the lee slope. The front of this gradually moves upstream, passing the dye port at $16 < \tau < 32$ (between panels 12 and 13, figure 15; a similar range of values was found for experiments at different *Re*, consistent with the observations of the dye-free zone shown in figure 12), and the separated eddy gradually settles down into its steady configuration ($\tau \approx 75$; figure 12).

The bead observations (figure 13) are consistent with the same interpretation, although they tell us more about the occurrence of reversed flow than about the recirculating vortex. It is interesting that the cores of rapidly moving beads starts approximately halfway between the two walls, as one would expect while boundary-layer theory remained valid near the walls (Smith 1976*a*, *b*), before the separated eddy on the indentation grows and distorts the flow asymmetrically.

However, the earlier experiments in which dye is introduced across much of the cross-section of the channel are much more difficult to interpret (figures 10 and 11). Vortices arise at the outside edges of the boundary layers at about the same time that flow reversal occurs at the walls. Now the above observations show that the flow next to the wall is not greatly disturbed, which suggests that these vortices are not part of the process of boundary-layer separation. Two possible explanations come to mind. One is that these disturbances are triggered off when a true separation eddy begins at the sharp concave corner downstream, and causes pressure perturbations upstream. Such pressure perturbations would also affect the boundary layer, of course, and would temporarily add to the adverse pressure gradient experienced in it, more readily promoting wall shear reversal. The other interpretation, already referred to in §3, is that the vortices are a manifestation of inflexion-point instability associated with the velocity profile in the adverse pressure gradient. These flow-visualization studies do not enable us to distinguish between the two possibilities. We should note, however, that similar vortices were observed at the outside edge of the boundary layer on an airfoil whose pitch angle was increasing, by McAlister & Carr (1979). They observed the vortices after flow reversal had spread over most of the airfoil surface (without boundary-layer thickening) but before significant leading-edge separation (the 'dynamic stall' that they were primarily investigating) had taken place. These authors referred to them as 'shear-layer vortices', indicating that they regarded them as the result of instability; certainly there was no downstream eddy to trigger off outer-flow pressure perturbations in their experiment. Their results add weight to our view that the vortices are not an intrinsic part of boundary-layer separation.

Turning now to the pressure measurments, summarized in figure 22, we note that the maximum value of the discrepancy between the predicted and the measured values of Δp_{47} is about $1.7\rho\bar{u}_0^2$ for the lowest *Re* and about $1.4\rho\bar{u}_0^2$ for the highest (the difference cannot be regarded as significant in view of the experimental scatter). These numbers are in good agreement with the value of $1.5\rho\bar{u}_0^2$ that one would expect if immediately after the flow has begun all the dynamic head at the constriction is recovered downstream and if, in the steady state, it is all lost. Now we know from

figures 7 and 8 that it is not all lost in the steady state, and in fact there is a pressure recovery ($-\Delta p_{47}$) that falls from about $0.32\rho\bar{u}_0^2$ at $Re = 1800$ to $0.16\rho\bar{u}_0^2$ at $Re = 500$ and below (these numbers are taken from the direct measurements of Δp_{47qs} rather than from figure 7). These values are fortunately not very large, and the consequent prediction that the peak in figure 22 should lie between $1.5\rho\bar{u}_0^2$ and $1.2\rho\bar{u}_0^2$ is still in reasonable agreement with the experimental results.

No detailed theory has yet been carried out to predict the time course of the pressure measurements of figure 22 (although the early stages of the growth and modification of Rayleigh layers can no doubt be modelled as for external flow; for example in the manner of Collins & Dennis 1973*a*). If the steady flow rate were established instantaneously, and if the resolution of the measurement system were perfect, then the peak in figure 22 would occur at $\tau = 0$. However, the flow rate takes a finite time to become established, as can be seen from figure 19, where the eventual constant slope of the curves is not achieved until times corresponding to values of τ between 1.8 and 3.2. Thus the appearance of the peak around $\tau = 2.5$ has no fluid-mechanical significance.

The time $\tau \approx 7$–10 for decay of the pressure discrepancy of course does have fluid-mechanical significance. It shows that the energy dissipation associated with separation reaches its steady-state value significantly before the flow patterns become stationary ($\tau \approx 75$; figure 12). According to the flow-visualization studies, $\tau = 7$ represents a time shortly after the thick separation eddy has formed and has begun to move upstream along the lee slope. Thus the unsteady pressure discrepancy falls most rapidly as the eddy is forming, i.e. as the width of channel available to the core flow is diminishing most rapidly. It is probable that the postulated inflexion-point instability leads to the turbulence responsible for most of the energy dissipation. In the context of flows in tubes or channels with oscillating walls, we should note that an oscillation whose Strouhal number St equals 1 has a period corresponding to $\tau = 2\pi$. This is close to 7, and confirms that the dissipative pressure drop will be quasi-steady only for much smaller values of St.

We are grateful to Dr S. J. Cowley and Dr F. T. Smith for their helpful advice concerning the theory of §3.3, and to Dr Cowley for integrating the boundary-layer equations for us. We are also grateful to the Science and Engineering Research Council for its financial support.

REFERENCES

Åström, K. J. & Eykhoff, P. 1971 System identification – a survey. *Automatica* **7**, 123–162.

Batchelor, G. K. 1967 *An Introduction to Fluid Dynamics*. Cambridge University Press.

Bertram, C. D. 1982 Two modes of instability in a thick-walled collapsible tube conveying a flow. *J. Biomech.* **15**, 223–224.

Bertram, C. D. & Pedley, T. J. 1982 A mathematical model of unsteady collapsible tube behaviour. *J. Biomech.* **15**, 39–50.

Bonis, M. 1979 Écoulement visqueux permanent dans un tube collabable elliptique. Thèse de Doctorat d'État, Université de Technologie de Compiègne.

Bouard, R. & Coutanceau, M. 1980 The early stage of development of the wake behind an impulsively started cylinder for $40 < Re < 10^4$. *J. Fluid Mech.* **101**, 583–607.

Cebeci, T. 1979 The laminar boundary layer on a circular cylinder started impulsively from rest. *J. Comp. Phys.* **31**, 153–172.

Collins, W. M. & Dennis, S. C. R. 1973*a* The initial flow past an impulsively started circular cylinder. *Q. J. Mech. Appl. Maths* **26**, 53–75.

COLLINS, W. M. & DENNIS, S. C. R. 1973*b* Flow past an impulsively started circular cylinder. *J. Fluid Mech.* **60**, 105–127.

CONRAD, W. A. 1969 Pressure-flow relationships in collapsible tubes. *IEEE Trans. Biomed. Engng* **16**, 284–295.

COWLEY, S. J. 1983 Steady flow through distorted rectangular tubes of large aspect ratio. *Proc. R. Soc. Lond.* **A385**, 107–127.

KOROMILAS, C. A. & TELIONIS, D. P. 1980 Unsteady laminar separation: an experimental study. *J. Fluid Mech.* **97**, 347–384.

MCALISTER, K. W. & CARR, L. W. 1979 Water tunnel visualisations of dynamic stall. *Trans. ASME* I: *J. Fluids Engng* **101**, 376–380.

PEDLEY, T. J. 1980 *The Fluid Mechanics of Large Blood Vessels.* Cambridge University Press.

PROUDMAN, I. & JOHNSON, K. 1962 Boundary layer growth near a rear stagnation point. *J. Fluid Mech.* **14**, 161–168.

SCHLICHTING, H. 1968 *Boundary Layer Theory*, 6th edn. McGraw-Hill.

SEARS, W. R. & TELIONIS, D. P. 1975 Boundary-layer separation in unsteady flow. *SIAM J. Appl. Maths* **28**, 215–235.

SECOMB, T. W. 1979 Flows in tubes and channels with indented and moving walls. Ph.D. thesis, Cambridge University.

SMITH, F. T. 1974 Boundary layer flow near a discontinuity in wall conditions. *J. Inst. Maths Applics* **13**, 127–145.

SMITH, F. T. 1976*a* Flow through constricted or dilated pipes and channels: Part 1. *Q. J. Mech. Appl. Maths* **29**, 343–364.

SMITH, F. T. 1976*b* Flow through constricted or dilated pipes and channels: Part 2. *Q. J. Mech. Appl. Maths* **29**, 365–376.

SMITH, F. T. 1977 Upstream interactions in channel flows. *J. Fluid Mech.* **79**, 631–655.

SMITH, F. T. & DANIELS, P. G. 1981 Removal of Goldstein's singularity at separation, in flow past obstacles in wall layers. *J. Fluid Mech.* **110**, 1–37.

SMITH, F. T. & DUCK, P. W. 1980 On the severe non-symmetric constriction, curving or cornering of channel flows. *J. Fluid Mech.* **98**, 727–753.

UR, A. & GORDON, M. 1970 Origin of Korotkoff sounds. *Am. J. Physiol.* **218**, 524–529.

WALKER, J. D. A. 1978 The boundary layer due to rectilinear vortex. *Proc. R. Soc. Lond.* **A359**, 167–188.

YOUNG, D. F. & TSAI, F. Y. 1973*a* Flow characteristics in models of arterial stenosis – I. Steady flow. *J. Biomech.* **6**, 395–410.

YOUNG, D. F. & TSAI, F. Y. 1973*b* Flow characteristics in models of arterial stenosis – II. Unsteady flow. *J. Biomech.* **6**, 547–559.